

# Discovering stochastic dynamical equations from biological time series data

Arshed Nabeel,<sup>1,2,\*</sup> Ashwin Karichannavar,<sup>2</sup> Shuaib Palathingal,<sup>2</sup> Jitesh Jhawar,<sup>3,4,†</sup> David B. Brückner,<sup>5</sup> Danny Raj M.,<sup>6</sup> and Vishwesh Guttal<sup>2,‡</sup>

<sup>1</sup>IISc Mathematics Initiative, Indian Institute of Science, Bengaluru, India

<sup>2</sup>Center for Ecological Sciences,

Indian Institute of Science, Bengaluru, India

<sup>3</sup>University of Konstanz, Konstanz, Germany

<sup>4</sup>Max Planck Institute of Animal Behaviour, Konstanz, Germany

<sup>5</sup>Institute of Science and Technology, Austria

<sup>6</sup>Department of Chemical Engineering,  
Indian Institute of Science, Bengaluru, India

(Dated: November 23, 2023)

Stochastic differential equations (SDEs) are an important framework to model dynamics with randomness, as is common in most biological systems. The inverse problem of integrating these models with empirical data remains a major challenge. Here, we present a software package, PyDaDDy (Python Library for Data Driven Dynamics) that takes time series data as an input and outputs an interpretable SDE. We achieve this by combining traditional approaches from stochastic calculus literature with state-of-the-art equation discovery techniques. We validate our approach on synthetic datasets, and demonstrate the generality and applicability of the method on two real-world datasets of vastly different spatiotemporal scales: (i) collective movement of fish school where stochasticity plays a crucial role, and (ii) confined migration of a single cell, primarily following a relaxed oscillation. We make the method available as an easy-to-use, open-source Python package, **PyDaddy** (Python Library for Data Driven Dynamics).

Keywords: Data Driven Model Discovery, Langevin Dynamics, Self-organisation, Collective motion, Mesoscale dynamics, Data Driven Dynamical Systems, Scientific Machine Learning, Noise induced order

## INTRODUCTION

A central approach to modelling complex dynamical systems across fields is via differential equations (Strogatz 2018, Gotelli *et al.* 2008). Depending on the importance of space and stochasticity in the system, these equations can be ordinary, stochastic, or partial differential equations. Even when we begin with a simple set of rules or interactions at a fine, local scale, one can derive coarse-grained dynamical descriptions, at levels such as groups, populations or even ecosystems, in the form of differential equations (McKane and Newman 2004, Cheng *et al.* 2014, Yates *et al.* 2009, Loreau 2010, Durrett and Levin 1994, Biancalani *et al.* 2014, Jhawar *et al.* 2019, Majumder *et al.* 2021). While such dynamical system based approaches are powerful and have provided key biological insights, how to meaningfully integrate empirical data with differential equation models continues to remain a challenge.

We are in the era of big data, where high-resolution data capturing the dynamics of biological systems is increasingly available (Leyk *et al.* 2019, Nathan *et al.* 2022). Examples span across scales of biological organisation, from individual (cells or animals) movement trajectories (Nathan *et al.* 2022) and group properties (Yates *et al.*

2009, Jhawar *et al.* 2020, Tunstrøm *et al.* 2013) to population sizes (Stenseth *et al.* 1997, Bjørnstad and Grenfell 2001), fitness of populations (Lenski 2017) and ecosystem states (Carpenter *et al.* 2020, Xie *et al.* 2008, Majumder *et al.* 2019). Importantly, data maybe available with high temporal resolutions, sometimes even across space, thus opening avenues for better integration between models and data.

To capture the dynamics of biological systems accurately, one has to treat state variables as nonlinear as well as stochastic, rather than accounting only for the linear and average properties. A suitable framework for analysing such myriad stochastic effects is via *stochastic differential equations (SDEs)*, which allows us to capture both the deterministic and stochastic factors driving the dynamics. Using SDE models, the most commonly understood effect of noise is that of creating fluctuations around a deterministic stable state. This is akin to a population fluctuating around its carrying capacity equilibrium due to environmental noise. However, the SDE models also predict that when the strength of the noise depends on the state of the system – also called state-dependent noise – it can create new states away from the deterministic stable equilibria (Horsthemke and Lefever 1989). For example, in fish schools systems, fluctuations associated with small group sizes, counter-intuitively, pushes the system away from deterministically stable disordered states; consequently, the group level coordination among fish increases (Biancalani *et al.* 2014, Jhawar *et al.* 2019, 2020). In the context of dryland ecosystems, rainfall fluctuations may create a new state

\* arshed@iisc.ac.in

† Now at: School of Arts and Sciences, Ahmedabad University, Ahmedabad, India.

‡ guttal@iisc.ac.in

between two deterministic stable states (D’Odorico *et al.* 2005). These examples illustrate the importance of determining the relative roles of deterministic and stochastic effects given real datasets.

Hence, we naturally focus on the following inverse problem: can we construct SDE models starting from observed time series datasets? Indeed, the answer is in the affirmative. Approaches based on estimating the so-called *jump moments*, in principle, allow us to infer stochastic differential equations from time series data (Gradišek *et al.* 2000, Friedrich *et al.* 2011, Tabar 2019, Jhavar and Guttal 2020, Rinn *et al.* 2016). Furthermore, in the context of deterministic models, recently developed *equation discovery* techniques allow us to infer parsimonious, interpretable differential equation models from time series data (Brunton *et al.* 2016, Rudy *et al.* 2017, de Silva *et al.* 2020). Recently, these techniques have been also extended for stochastic dynamical systems (Boninsegna *et al.* 2018, Huang *et al.* 2022, Callahan *et al.* 2021, Frishman and Ronceray 2020, Brückner *et al.* 2020). These approaches are promising for analysing biological time series datasets.

However, there are significant gaps. These techniques are scattered across physics and engineering literature; they are thus not well known in biological contexts. Importantly, there is no fundamental reason to believe that SDEs which assume relatively simple noise structures are reasonable models for real biological datasets. Therefore, proper diagnostic tools that test the assumptions of noise and validate the correct model are essential; however, such diagnostics are often not the focus in the physics and engineering literature where many of these new techniques are being developed. Consequently, the methods of stochastic equation discovery are currently not readily amenable for biological applications.

In this manuscript, we bridge these gaps and present a unified framework for discovering and diagnosing SDE models for biological datasets. Put simply, our approach allows a user to input a time series and discover an underlying stochastic differential equation. We argue that this approach is powerful, since it allows us to extract parsimonious and interpretable SDE models directly from data. Equation learning approach is different from traditional curve-fitting and parameter estimation; equation learning *discovers* an appropriate functional form of the model the given data with minimal input from the user; and not merely estimate the parameters of a user defined function. We demonstrate the generality of our approach via a number of applications: (A) We deliberately choose SDEs where deterministic and stochastic terms are fundamentally different; however, the parameters of these contrasting SDEs are so chosen that they produce very similar times series. We then show that we can recover the underlying equations (SDEs) accurately from time series data alone. (B) We then apply the method to two previously published real world datasets having contrasting scales and dynamics:

(i) a schooling fish movement driven by stochasticity, and (ii) a single cell movement driven by a deterministic limit cycle with a minimal role of stochasticity. For these datasets, we show that our approach can discover underlying SDEs which capture the features of data accurately. To make our approach widely accessible, we provide our open-source codes via a package named **PyDaDDy** (Python library for **Data Driven Dynamics**). The package takes a time series of a state variable (scalar or vector) as the input, and outputs an interpretable SDE model, together with a number of jupyter notebooks, visualization and diagnostic utilities. The tool can be accessed even without installation via Google Colab: <https://pydaddy.readthedocs.io/en/latest/tutorials.html>.

## RESULTS

### The basic principle: combining jump moments and equation learning

Consider a time series of some observed variable, denoted as  $x$ , such as population size or a measure of group’s movement, available at a high temporal resolution. We wish to discover an equation governing the dynamics of  $x$ , capturing both the deterministic and stochastic aspects. This can be done using a stochastic differential equation of the form,

$$\dot{x} = f(x) + g(x)\eta(t) \quad (1)$$

(interpreted in the *Itô sense*) that describes the temporal dynamics of  $x$ . Here,  $f$  and  $g$  are functions of  $x$ , and  $\eta(t)$  is Gaussian white-noise (Gardiner 2009).

Eq. 1 describes how the rate of change of  $x$  depends on the instantaneous value of  $x$ . The average rate of change of  $x$  over time is governed by  $f$ , called the deterministic or *drift* function. The fluctuation around the average value is governed by  $g^2$ , called the stochastic or *diffusion* function. When  $g$  is a constant (i.e. independent of  $x$ ), the strength of the noise is the same for all values of  $x$ , and is called *additive* or *state-independent* noise. When  $g$  is a function of  $x$  (and not a constant), the strength of the noise depends on the instantaneous value of  $x$ , and is called *multiplicative* or *state-dependent* noise (Horsthemke and Lefever 1989).

Our goal is to discover the drift ( $f$ ) and diffusion functions ( $g^2$ ) from the observed time series data. Specifically, we aim to find simple, interpretable analytical expressions that describe  $f$  and  $g^2$ , not just the qualitative shape. Our approach to this problem involves two steps (see *Methods* section for the a more detailed mathematical description of the procedure):

1. First, we extract the drift and diffusion components from the given time series data, using the so-called *jump moments* or the *Kramer-Moyal coefficients* (Tabar 2019)).

- Next, we use a technique based on sparse regression, sometimes referred to as *equation learning*, to find interpretable analytical expressions of the extracted drift and diffusion functions (Brunton *et al.* 2016, Boninsegna *et al.* 2018).

We emphasise the technical novelty of our approach described above. Conventional SDE estimation approaches usually stop with the first step. The drift and diffusion functions are estimated as binned averages, based on user input values of bin sizes and sampling time; although studies provide some rules of thumb for selecting these parameter values, the results can dramatically vary if incorrect values are given (Jhawar and Guttal 2020). Besides, the estimates are often noisy, especially when the observed time series is short. By combining the conventional approach with sparse-regression-based equation discovery techniques, our approach precludes the need of arbitrary parameter choices while also improving the accuracy of the estimates. Additionally, the equation-learning step uses cross-validation to select an appropriate parsimonious model, where the goal is to choose a model that achieves the best trade-off between cross-validation error and model complexity (see *Methods*, section *Model selection for sparse regression*).

### Diagnosics

Modelling a given time series using an SDE is contingent on several assumptions. Therefore, the data-driven SDE discovery pipeline is incomplete without sufficient diagnostic tests to make sure that the underlying assumptions are reasonably satisfied. Extending ideas from (Jhawar and Guttal 2020, Brückner *et al.* 2019), we propose two sets of diagnostic tests that enable evaluation of the discovered SDE model.

- *Noise diagnostics.* The noise term  $\eta(t)$  in Eq. 1 is assumed to be uncorrelated Gaussian noise. The residual, defined as  $r(t) = [\dot{x}(t) - F(x(t))] / \sqrt{G(x(t))}$  where  $F$  and  $G$  are the estimated drift and diffusion functions, is an estimate of  $\eta(t)$  and should have a standard normal distribution. For a vector time series, the residuals should also be isotropic, i.e. the vector components of the residuals should be uncorrelated. The residual  $r(t)$  should also be uncorrelated across time.
- *Model diagnostics.* Suppose we estimate an SDE model using our approach. If we generate a simulated time series using this estimated model, with identical length and sampling interval as the original time series, then the simulated time series should have the same probability distribution and autocorrelation function as the original time series. We note that these two properties of the data were

not used as part of the data-driven model discovery procedure. Further, if we subsequently estimate an SDE model from this simulated time series, we must recover the same model.

Our proposed SDE discovery protocol incorporates both the noise and the model diagnostics to ensure that the data-derived model reasonably describes the real-biological process at hand. More advanced diagnostic tests are possible to check detailed assumptions of the SDE model—these are described in more detail in *Methods* (section *Advanced diagnostics*), and implemented in the package.

### PyDaDDy – an open-source package for data-driven SDE discovery

We make the above SDE estimation procedure available via an easy-to-use open-source python package named **PyDaDDy** (**P**ython library for **D**ata **D**riven **D**ynamics). Figure 1 shows an overview of the package. Appendix A presents a brief walk-through of the package and its key features. Code that implement the workflow are available as Jupyter notebooks as a part of our open-source package. In addition, we also provide a number of other notebooks to analyze model simulated data to illustrate usage as well as various features of the package.

We now evaluate the method on systems where the ground-truth governing dynamics, i.e. SDEs, are known. We then apply our method to two (previously published) real world datasets of contrasting scales and dynamics.

### Discovering contrasting SDEs from synthetic datasets

#### *Unimodal distributions from contrasting SDEs*

Unimodal distributions are widely observed in many biological datasets. However, they may be generated from very different dynamical processes and thus can be modelled by contrasting underlying SDEs. Our aim here is to show that even in such cases, we can discover the original SDEs by applying our proposed method to the time series data. We consider the following two SDEs:

$$\dot{x} = -x + \sqrt{2} \cdot \eta(t) \quad (2)$$

$$\dot{x} = x - x^3 + 2 \left( \sqrt{1 + x^2} \right) \cdot \eta(t) \quad (3)$$

Although Eq. 2 and 3 are quite different, the time series generated with these equations as well as their histograms are very similar (Fig. 2 (A-i, A-ii, B-i, B-ii)): in fact, the steady-state distributions of  $x(t)$  are unimodal

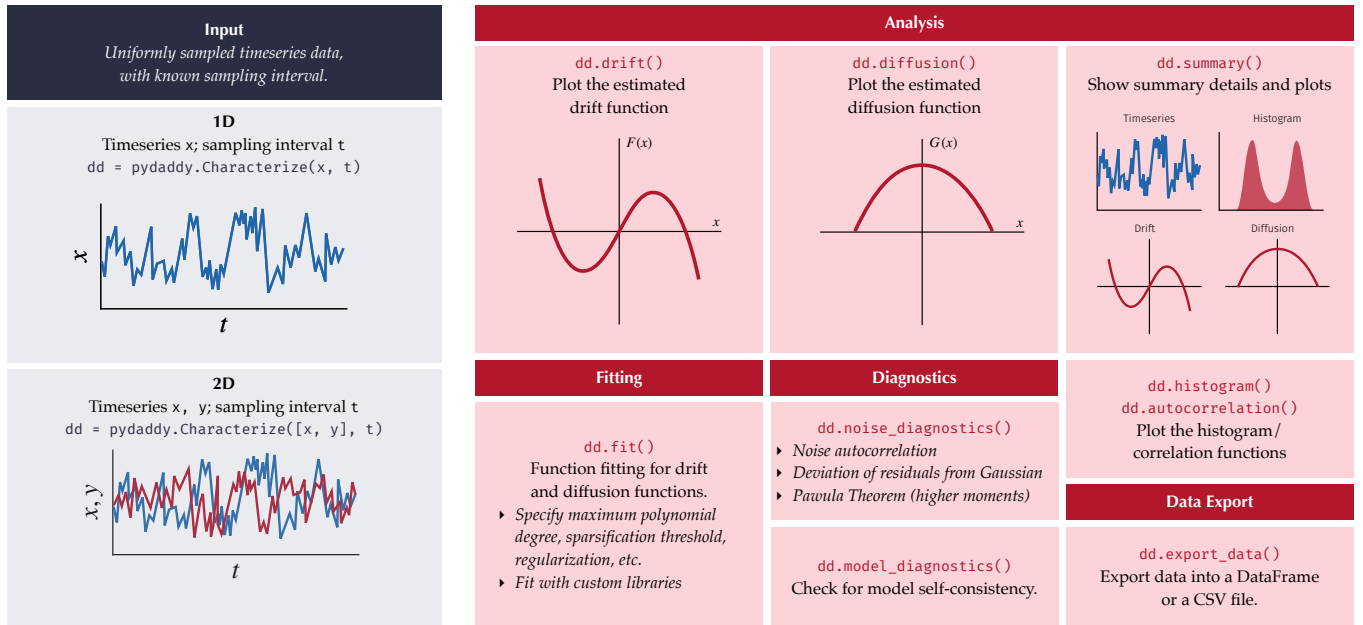


FIG. 1. **Overall schematics of the PyDaDDy package.** PyDaDDy takes as input uniformly sampled 1D or 2D time series, and computes the drift and diffusion components from the time series. Several functions are provided to visualize data as time series or histograms, fit drift and diffusion functions, diagnose whether underlying assumptions for drift-diffusion estimation are met, and to export data.

and are nearly identical for Eq. 2 and 3. From a dynamical systems point of view, Eq. 2 has a single deterministic stable state at  $x^* = 0$ . Biologically,  $x$  could be thought of as the deviation of the population size from its stable carrying capacity. Therefore,  $x$  could be positive or negative. The additive noise—representing environmental fluctuations—simply spreads the dynamics of the population around the deterministic equilibrium, as reflected in the time series as well as histogram (Fig. 2 (A-ii)). Therefore, we may refer to the mode of the histogram as reflecting a *deterministic state*. This is indeed the most commonly understood effect of noise.

On the other hand, for Eq 3 the deterministic stable equilibria are at  $\pm 1$  but the mode of the histogram is at 0 (Fig. 2 (B-ii)). In this case, the state-dependent noise or the multiplicative noise-term completely alters the stability landscape, creating a new state between two deterministic stable states, leading to a mode at  $x = 0$ . This is an example of an unusual effect of noise, called the noise-induced stable state proposed in a dryland ecosystem model (D’Odorico *et al.* 2005).

For these unimodal datasets, we now pose the inverse problem: can we infer the correct underlying SDE models based on the features the time series data (Fig. 2 A-i versus B-i). Indeed, our approach that integrates jump moment computations with sparse regression accurately identifies the functional forms of the drift and diffusion for both the models (in Fig. 2 compare red and black lines within columns A and B; rows iii and iv). Crucially, we are able to infer that the time series of Fig. 2 A-i is governed by a linear drift (Fig. 2 A-iii) with an

additive noise (Fig. 2 A-iv); in contrast, the time series of Fig. 2 B-i is driven by a nonlinear drift function with three roots (Fig. 2 B-iii) and a multiplicative noise (Fig. 2 B-iv). Furthermore, we are also able to recover the symbolic analytical expressions for the drift and diffusion functions which closely match the original SDEs that we deployed to generate the synthetic datasets (Fig. 2, ‘Estimated’ panel).

#### Bimodal distributions from contrasting SDEs

Many biological systems exhibit alternative stable states, the simplest case being a bistable system, e.g. grassland and woodland states in dryland ecosystems or eutrophic and oligotrophic states of lakes. Systems with bistability show bimodal distributions of their state variable. Here too, bimodality can be generated by contrasting underlying processes/SDEs. To illustrate this, we consider the following two toy models:

$$\dot{x} = 2x - 3x^3 + \frac{1}{2} \cdot \eta(t) \quad (4)$$

$$\dot{x} = -x + \sqrt{2}(1 - x^2) \cdot \eta(t) \quad (5)$$

Eq. 4 has two deterministic stable equilibria at  $\pm \sqrt{2/3}$ , and the dynamics is spread around these equilibria by the additive noise (Fig. 2 (C-ii)); thus, these are deterministic states. On the other hand, Eq. 5 has only one stable equilibrium at  $x^* = 0$ ; yet, due to the effect of

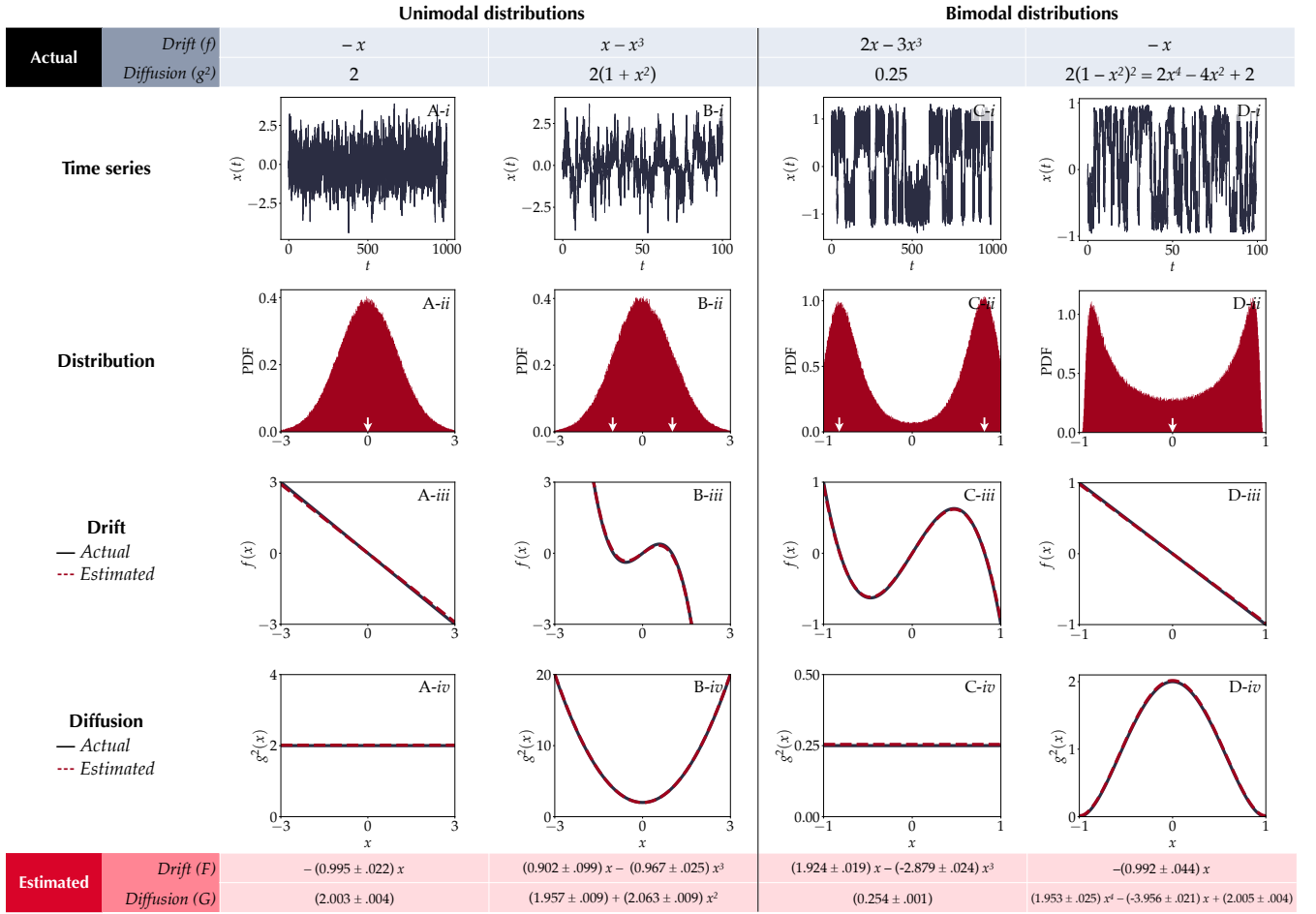


FIG. 2. Sparse regression on the extracted instantaneous jump moments reliably reconstructs governing equations from simulated data, for a wide range of dynamics. The mathematical expressions for the actual and estimated drift and diffusion functions are shown in the tables on the top (grey shaded) and bottom (red shaded), respectively. Row  $i$  shows a sample of the time series  $x(t)$  of the models Eqs 2-5, respectively, across four columns (A-D), while row  $ii$  shows the corresponding histograms of  $x(t)$ . The arrows in histograms in (A) and (B) mark the deterministic stable equilibria of the respective systems. Notice that the histograms in (A) and (B) are nearly identical, despite the underlying SDEs being very different. Similarly, the histograms in (C) and (D) are similar. (A) A ‘deterministic’ unimodal system (from Eq 2). (B) A ‘noise-induced’ unimodal state (from Eq. 3). (C) A ‘deterministic’ bimodal system from Eq. 4), with noise facilitating transitions between two deterministic states. (D) A ‘noise-induced’ bimodal state (from Eq. 5). Rows  $iii$  and  $iv$  compare the ground-truth (black) drift and diffusion functions with the estimated ones. The functions estimated using sparse regression are shown as dark red dashed lines. In all cases, the proposed method accurately recovers the drift and diffusion functions.

the multiplicative noise term, the system exhibits two modes in the histogram away from the deterministic equilibrium (Fig. 2 (D-ii)); thus, these are noise-induced states.

We again pose the inverse problem for these bimodal time series datasets (Fig. 2 C-i versus D-i and Fig. 2 C-ii versus D-ii). Here too, our method is able to recover the underlying SDE model correctly. Specifically, we find that for the data corresponding to Fig. 2 C-i, the drift is a nonlinear function with three roots (Fig. 2 C-iii) where as the noise is additive (Fig. 2 C-iv). On the other hand, for the data corresponding to Fig. 2 D-i, the drift is a linear function (Fig. 2 D-iii) whereas the diffusion is a nonlinear function of  $x$  which is maximum at  $x = 0$  (Fig. 2

D-iv). Furthermore, we are also able to recover the functional forms of the underlying SDEs which match well with the functions we actually used to generate the synthetic data (Fig. 2, ‘Estimated’ panel).

### Demonstration with classical models in theoretical biology

Having demonstrated that the SDE discovery procedure can accurately discover underlying SDEs for contrasting underlying dynamics, we now validate the method against several classical models in theoretical biology. We considered stochastic modifications a variety of models, with both one and two variables. The fol-

lowing univariate models were considered: the logistic model of density dependent population growth, a population harvesting model with a Hollings type III functional response, and a lake eutrophication model (Carpenter *et al.* 1999) showing bistability. The bivariate models considered were: the Lotka-Volterra competition model for inter-specific competition, and a non-linear predator-prey model with a Holling’s type II functional response for predation (Alonso *et al.* 2002), and the Van der Pol oscillator, a minimal model for non-linear oscillations. The stochastic noise terms considered in these models were usually multiplicative in nature.

Details of this analysis is summarized in Appendix B. In summary, for all the models considered, the SDE discovery procedure was able to accurately discover the correct model from simulated time series. Next, we move on to apply the SDE discovery techniques to discover governing equations from real-world datasets.

### Application to real datasets

At the outset, it is not obvious that these methods are applicable for complex biological datasets. In particular, SDEs assume a Gaussian uncorrelated noise while we often expect more complicated noise structure (e.g., non-Gaussian and with memory) for real datasets. Therefore, we demonstrate the applicability and generality by using them on two contrasting datasets, a dataset of group trajectories of schooling fish (Jhawar *et al.* 2020), and another of confined single-cell migration (Brückner *et al.* 2019).

The two datasets are different in many important ways. First, the fish schooling dataset captures emergent group-level order, while the cell dataset is an individual level behaviour. Second, the fish school has a relatively spatial span ( $\sim 1$  m), but has relatively fast temporal dynamics ( $\sim 0.1$  s). In contrast, the cell dataset has a small spatial span ( $\sim 10^{-4}$  m) but the cells move very slowly, with a timescale of 10 min. Finally, their underlying dynamics are fundamentally different—while fish schools are in a noise-induced state, the cell movement is predominantly a deterministic limit cycle with noise playing a minor role.

#### *SDE discovery of noise-induced schooling of fish*

Among various fields of biology, the field of collective animal motion has advanced substantially over the last decade. Employing the state of the art imaging technologies to record moving collectives, researchers have produced highly resolved spatiotemporal datasets that helps us probe into the mechanistic origins of the synchronized collective motion. Mathematical theories of flocking express the dynamics of collective motion in the form of stochastic differential equations—offering

potential explanations for such synchronous group dynamics (Biancalani *et al.* 2014, Jhawar *et al.* 2019, Vicsek and Zafeiris 2012, Toner *et al.* 2005, Ramaswamy 2017). With the availability of high-quality animal movement data, we now pose the inverse problem, i.e. can a stochastic dynamical model be discovered from given time series of animal trajectories? Further, one can address fundamental questions on the role of stochasticity in shaping (or destroying) the order. For example, is the observed collective dynamics consistent with a deterministic state (i.e. does stochasticity merely blur the order around a deterministic stable equilibrium as in Fig 2(A-ii)) or a noise-induced state (i.e. does stochasticity create nontrivial states away from the deterministic stable equilibrium, as in Fig 2(C-ii))?

A recent study inferred that highly synchronised motion of schooling fish is a noise-induced state (Jhawar *et al.* 2020). To do so, they employed the conventional jump moment estimation on the time series data of group dynamics. Here, we test if we can recover the same results using our inference protocol that integrates jump moment computation with the sparse regression. Further, we perform noise and model diagnostics, which was ignored in that study.

We use the openly available published dataset of a group of *Etroplus suratensis* (karimeen), from (Jhawar *et al.* 2020). Here, the motion of a school of 15 fish was recorded using a high-resolution camera and was subsequently tracked using computer vision methods. From the tracked individual trajectories, the degree of order of the collective motion was quantified via a two-dimensional *group polarisation* vector, denoted  $\mathbf{m} = (m_x, m_y)$ : This is simply the vector average of the directions of all fish, with the following interpretation. If the school of fish is highly ordered, with nearly all fish moving in the same direction, the magnitude of the polarisation vector,  $|\mathbf{m}|$ , will be close to 1. On the other hand, if the group is disordered, with fish moving in random directions,  $|\mathbf{m}|$ , will be close to 0. The dataset contains the time series of  $\mathbf{m}$ , which is available at a uniform interval of 0.12 second, for a duration of roughly one hour, with several missing data points (corresponding to time points where the tracking was imperfect). Although the time series of the group polarisation  $\mathbf{m}$  shows significant stochastic fluctuations (Fig 3B), the histograms show that the fish school is predominantly ordered (Fig 3C, D). This forms the input time series dataset for our analysis.

Here, we are able to recover the same results by using our protocol—implemented via the package PyDaDDy—that combines jump moment estimation and sparse regression. Our discovered equation contains a linear drift and a quadratic diffusion, with a vector SDE (in an *Ito* sense) of the form (see Appendix D for more details):

$$\dot{\mathbf{m}} = -\alpha\mathbf{m} + \sqrt{\beta(1 - |\mathbf{m}|^2)} \cdot \boldsymbol{\eta}(t), \quad (6)$$

with  $\alpha = 0.16$  and  $\beta = 0.26$ .

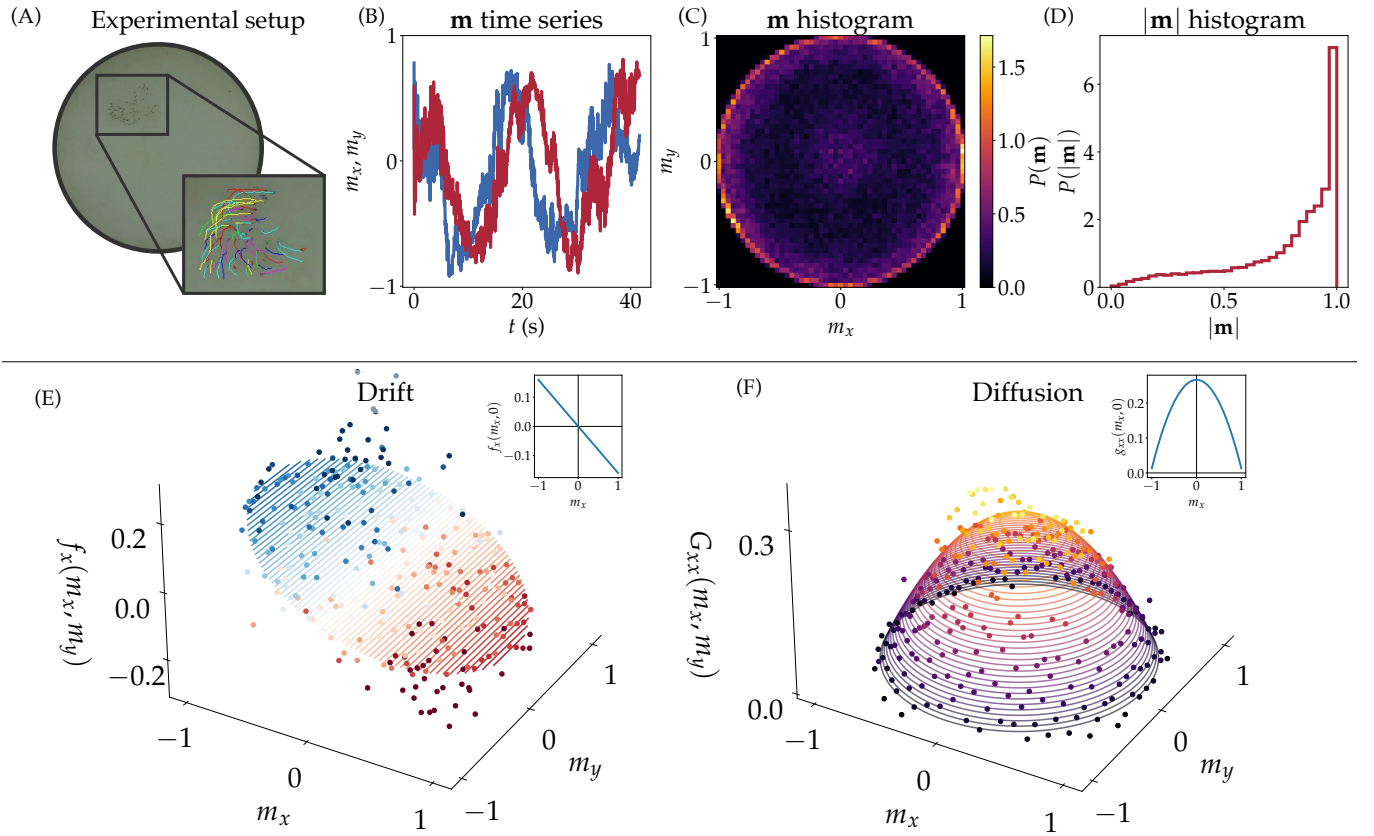


FIG. 3. **Data driven SDE discovery for polarisation dynamics in fish schools.** (A) Experimental setup. Individual fish trajectories are extracted from video recordings of fish swimming in a tank. (B) From the individual trajectories, a time series of the polarisation vector,  $\mathbf{m}$ , is computed. (C, D) Histograms of the polarisation vector,  $\mathbf{m}$  and the net polarisation,  $|\mathbf{m}|$ , respectively. (E) The drift function discovered by the SDE discovery procedure. The  $x$ -component of the function,  $f_x$  is shown. The surface plot shows the fitted drift function, and the points show the binwise averaged estimates. Inset shows a slice of this function along the  $y = 0$  plane, showing a single stable equilibrium at  $x = 0$  (F) The discovered diffusion function. Inset shows a slice along the  $y = 0$  plane. The diffusion is maximum at  $\mathbf{m} = 0$ , and decreases outwards.

The deterministic stable equilibrium of this data-discovered SDE is a disordered state, i.e.  $\mathbf{m}^* = 0$  (Fig 3E). However, the observed state, or the mode of the order parameter, is at  $|\mathbf{m}| \approx 1$ , away from the deterministic stable state. This leads to a striking, counter-intuitive implication that schooling fish is a noise-induced state (we refer the readers to (Jhavar *et al.* 2020) for further discussion on this intriguing phenomenon).

Fig. 4 shows the results from diagnostic tests on the discovered SDE model. The noise residual  $r(t)$  has a Gaussian distribution, as expected (Fig. 4A). The correlations in the residual noise  $r(t)$  decays rapidly (Fig. 4B). These tests reasonably support the modelling assumption of  $\eta$  being Gaussian white noise.

We also find that the discovered equations pass model diagnostic tests. The histogram of simulated SDE from Eq 6 closely matches the histogram of  $\mathbf{m}$  from the original time series 4C). The autocorrelation of the simulated time series also shows reasonable agreement with the original time series 4D), with one notable deviation: The data autocorrelation shows negative values over rela-

tively larger time scales of  $\approx 10$  s, before converging to zero. The authors of the fish schooling paper demonstrated that this feature arises from boundary effects that are unimportant for schooling dynamics of *Etroplus suratensis*. Nevertheless, we emphasize that the SDE discovery protocol used only highly local information of group polarisation fluctuations at very small time scales  $\approx 0.1$ s; it did not use any information on either the frequency distribution or the autocorrelation function of the group polarisation data. Despite this, the simulated time series shows a good agreement with data in both these metrics. Last, but not the least, we find that the model is self-consistent, with the same SDEs being recovered when we pass the simulated data via our equation discovery protocol.

#### SDE discovery for dynamics of confined cell migration

From morphogenesis and wound healing to cancer metastasis, cell migration plays a key role in many bio-



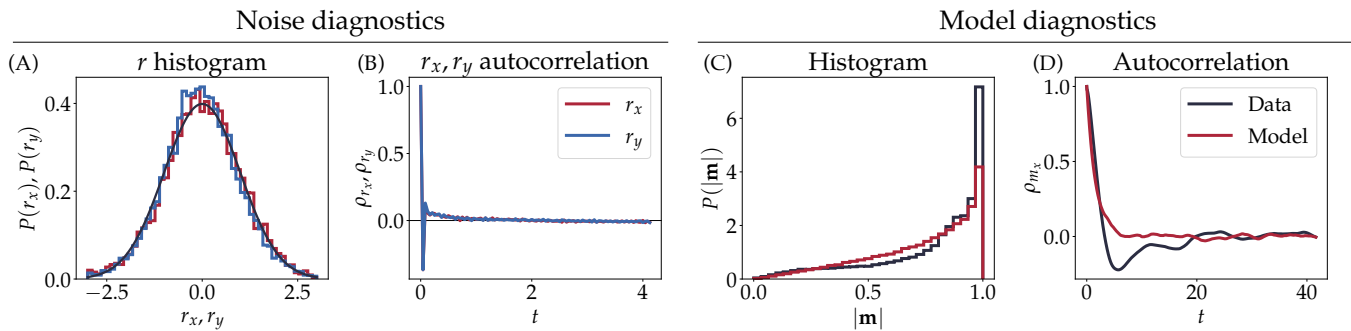


FIG. 4. **Diagnostics of the discovered SDE for polarisation dynamics.** (A, B) Noise diagnostics. (A) The histogram of the residual noise  $\eta$ , computed based on the discovered SDE. The  $\eta_x$  and  $\eta_y$  marginals are shown as red and blue. These should match a standard normal distribution, shown in black. (B) The autocorrelation functions of  $\eta_x$  and  $\eta_y$ . The autocorrelation should decay within one sampling time step. (C, D) Model diagnostics. (C) Histogram of  $|m|$  from the original time series (black) compared to that of a simulated time series generated from the discovered SDE (red). (D) Autocorrelation of the  $m_x$  component of the real (black) and simulated (red) time series.

logical contexts, where it is crucial to understand how cells move through complex environments. A recent study (Brückner *et al.* 2019) explored the stochastic dynamics of cell migration in structured environments. The authors designed an experiment where a cancerous cell migrates back and forth between two *islands* (‘states’) (Fig 5A), and modelled the dynamics of this two-state migration using an SDE framework, but without using an explicit expression. They concluded that the dynamics is primarily governed by a limit cycle in the deterministic (drift) component. The stochastic component plays a relatively minor role affecting only the timescale of the transition between states. Here, we reproduce the key results from this study using our SDE discovery protocol. While the original study represented the SDE using bin-averaged, piecewise representations of the drift and diffusion functions, our methodology enables us to extract interpretable functional forms. Further, we demonstrate how the noise and model diagnostics can lead to a more accurate model-discovery.

The dataset consists of 149 independent replicate cell trajectories. Each trajectory was based on high-resolution images taken once every 10 minutes, for a duration of up to 50 hours. Fig. 5B shows an example time series of the cell movement between the two islands and Fig. 5C-E depict histograms of the state variables (position  $x$  and velocity  $v$ ).

The dynamics of the cell can then be hypothesized to follow an underdamped SDE system given by:

$$\dot{x} = v \quad (7)$$

$$\dot{v} = f(x, v) + g(x, v) \cdot \eta(t) \quad (8)$$

Here, we scale  $x$  and  $v$  to non-dimensionalize them before applying the SDE discovery procedure. This is necessary for the sparse regression to work correctly, see Appendix D for details. Using our SDE discovery pro-

cedure, we find that the drift function  $f$  (Fig. 5E) is well approximated by a cubic polynomial of the form:

$$f(x, v) = \underbrace{(\alpha_1 - \alpha_2 x^2)v - \alpha_3 x}_{\text{Terms in Van der pol equation}} + \underbrace{\alpha_4 x^3 - \alpha_5 v^3 - \alpha_6 x v^2}_{\text{additional terms}} \quad (9)$$

with  $\alpha_1 = 49.84$ ,  $\alpha_2 = -3.50 \times 10^{-3}$ ,  $\alpha_3 = -1.27$ ,  $\alpha_4 = 5.51 \times 10^{-4}$ ,  $\alpha_5 = -2.01 \times 10^{-4}$ , and  $\alpha_6 = -1.49 \times 10^{-3}$ .

Further, we discover a multiplicative noise for the diffusion function  $g^2(x, v)$ , approximated to a 4th order polynomial of the form, (Fig. 5F).

$$g^2(x, v) = \beta_1 - \beta_2 x^2 + \beta_3 x^4 - \beta_4 x v + \beta_5 x^3 v - \beta_6 v^2 + \beta_7 x^2 v^2 + \beta_8 x v^3 + \beta_9 v^4, \quad (10)$$

with  $\beta_1 = 3.20 \times 10^4$ ,  $\beta_2 = -1.20 \times 10^{-2}$ ,  $\beta_3 = 1.25 \times 10^{-9}$ ,  $\beta_4 = -3.34 \times 10^{-3}$ ,  $\beta_5 = 6.53 \times 10^{-10}$ ,  $\beta_6 = -5.16 \times 10^{-5}$ ,  $\beta_7 = 8.13 \times 10^{-11}$ ,  $\beta_8 = 2.62 \times 10^{-12}$  and  $\beta_9 = -2.87 \times 10^{-14}$ .

The actual values of the coefficients, in both the scaled and unscaled coordinates, are shown in SI Tables S2 and S3 (Appendix D).

Our data-discovered SDE model of cell migration yields an excitable flow, qualitatively consistent with the findings of (Brückner *et al.* 2019), exhibiting relaxation oscillations. Furthermore, we see that the drift function deviates from the classic Van der Pol oscillator, which is a minimal model that explains for relaxation oscillations. Intriguingly, as shown in the Appendix D, we find that this diffusion term is necessary to capture the finite boundary effects on the dynamics of cell as well as to satisfy model diagnostics (see below).

Fig. 6 shows the diagnostic results of the discovered model. The noise residuals show no correlation in time (6B), but the distribution of the noise show deviations and has a stronger central tendency than a Gaussian distribution (6A). Nevertheless, the discovered model



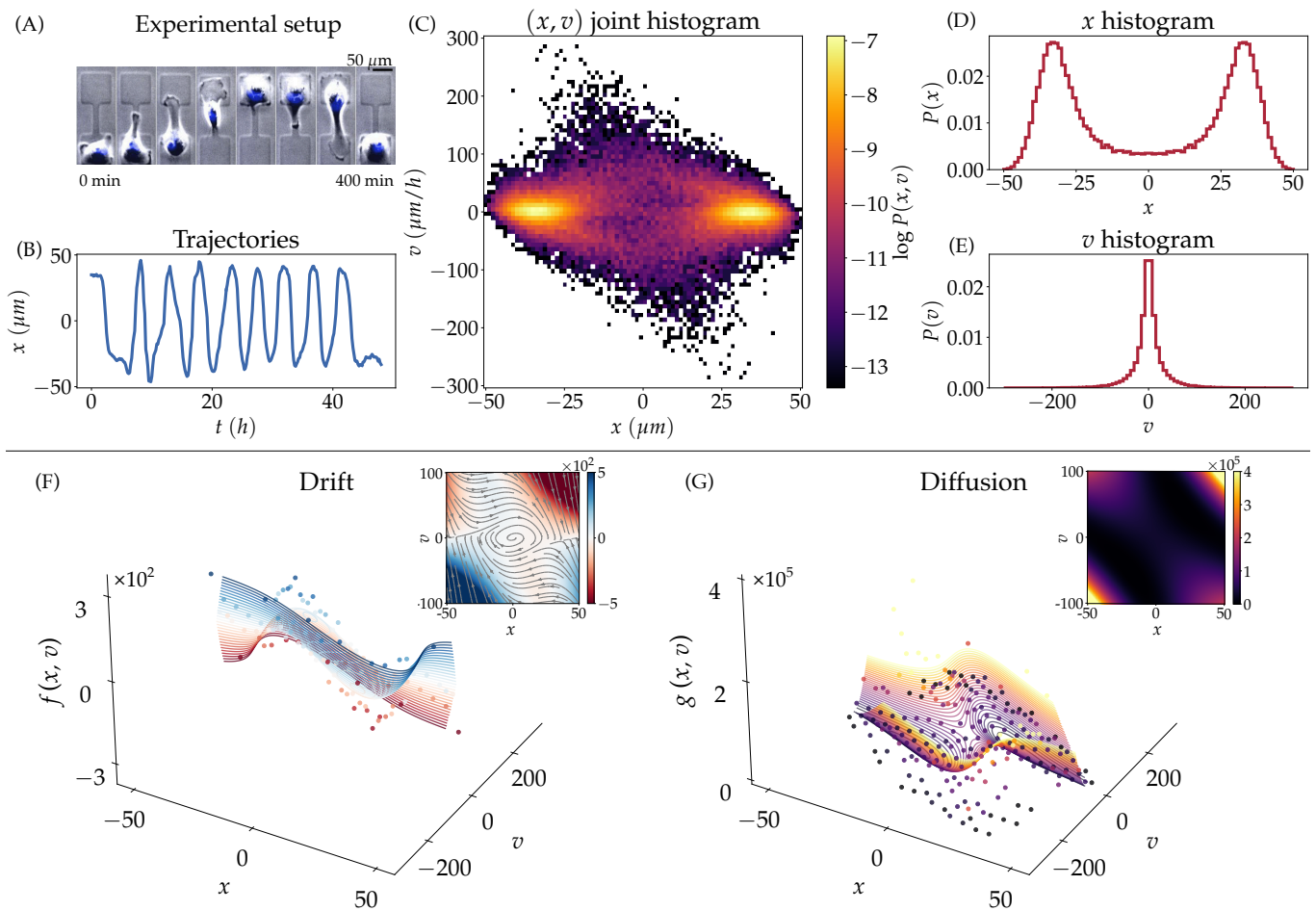


FIG. 5. **Discovering SDEs governing the dynamics of confined migration of cancer cells.** (A) The experimental setup, showing a micropattern with two landing pads, and the cell hopping between them. (B) Example time series of cell position. (C) Joint histogram of the position  $x$  and velocity  $v$  of the cell trajectories. (D, E) Marginal histograms of  $x$  and  $v$ . (F, G) The discovered SDE for the dynamics of  $v$ . (F) The drift function,  $f(x, v)$ . The surface plot shows the fitted drift function, and the points show the binwise averaged estimates. Inset shows the direction field of the deterministic dynamics, with the background colour denoting  $f$ . (G) The diffusion function,  $g(x, v)$ . Inset shows the diffusion as a colour map. Since  $g$  is relatively higher near the limit cycle, the actual observed cycles have slightly larger amplitude.

is able to produce simulated time series with statistical properties, i.e. state variable histograms and the auto-correlation functions, broadly consistent with the original data (6C-F). Additionally, the model we have presented is self-consistent. Here, we highlight the important role played by model diagnostics in the accurate discovery of the diffusion term. An additive noise term (i.e. a constant diffusion) with the same drift function could not accurately capture the spatial constraints of the cell migration, with the simulated trajectories frequently crossing the locations beyond the boundary. This led to huge discrepancies between the histogram of the state variables of data and the simulated model. However, a fourth order diffusion term was able to minimize such physical barrier violations; this enabled better model self-consistency. Therefore, we interpret that the diffusion term effectively captures spatial con-

straints.

## DISCUSSION

In this paper, we have presented a method that takes empirically observed time series as the input and discovers a data-driven stochastic dynamical equation in an analytically interpretable form. To achieve this, we combined the traditional approaches of drift and diffusion estimation using jump moments (Tabar 2019, Jhawar and Guttal 2020), with techniques based on sparse regression (Brunton *et al.* 2016, Boninsegna *et al.* 2018). Importantly, we emphasized the need for diagnostics to test the assumptions associated with data-derived models and the validity of the discovered model. In addition to illustrating the power and novelty

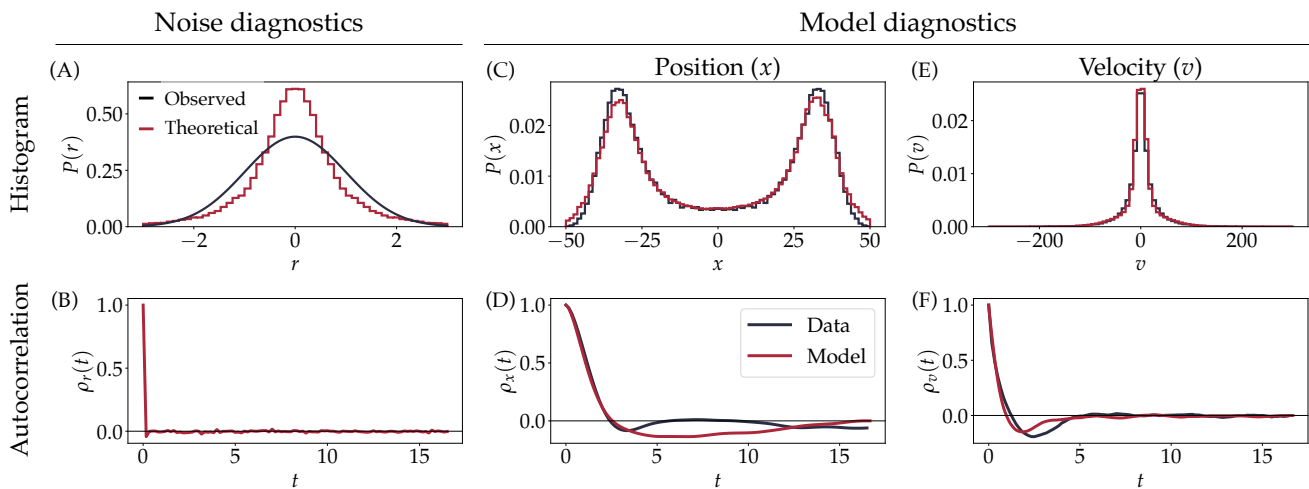


FIG. 6. **Diagnostics of the discovered SDE.** (A, B) Noise diagnostics. (A) The histogram of the residual noise  $r$ , computed based on the discovered SDE and data. This should match a standard normal distribution, shown in black. (B) The autocorrelation function on  $r$ . (C-F) Model diagnostics. (C, E) Histograms of the position and velocity of the original data (black) versus a time series simulated using the discovered model (red). (D, F) Autocorrelations functions of the position and velocity of the original data (black) versus a time series simulated using the discovered model (red).

of the method in synthetic datasets where the ground truth equations are known, we demonstrated the generality of the method with applications to two contrasting biological time series datasets—one of schooling fish and the other of cell migration.

We explain the novelty of our method, and how it can offer unique insights on the underlying dynamics of biological systems. Let us eye-ball the data of the group polarisation variables ( $m_x, m_y$  from Fig 3 A) from the schooling fish experiment and the cell migration data ( $x, v$  from Fig 5 A). Based on this, one may naively infer that they both seem to exhibit oscillatory patterns in their respective state variables, perhaps with different degrees of stochasticity. Some classic dynamical system based explanations for oscillations are that of a simple harmonic oscillator and a van der Pol oscillator, both of which are deterministic processes. One can also hypothesize more complex dynamical models/processes that offers explanations of the qualitative as well as the quantitative features of the data. However, based on the data-driven equation discovery, we discovered a stochastic dynamical equation which reveals that the schooling is a noise-induced state, formed away from the deterministic stable equilibrium. On the other hand, the oscillatory patterns of the cell data were revealed to be due to a deterministic limit cycle, with noise playing a relatively minor role. Furthermore, the mathematical structure of this limit cycle is different from that of a classic van der Pol oscillator. In other words, we could eliminate a number of alternative hypotheses while arriving at data-driven dynamical models with symbolic representations, with relatively minimal user inputs.

To enable the use of this powerful method to larger audience of biological researchers, we also include an open and easy to use Python package, Py-

DaDDy <https://pydaddy.readthedocs.io/>. In comparison with other packages of SDE modelling of time series data (see below), our approach is unique because it allows the user to *discover* an interpretable expression for the SDE. In addition, it includes comprehensive diagnostic and visual tools, features which are either limited or absent in other packages. Specifically, we have incorporated (i) noise diagnostics and (ii) the model consistency tests. We emphasize an important point here: although our integrated SDE estimation protocol provides functionality for automatic model selection, the model selection procedure works best when coupled with some human input based on theory and understanding of the system. In particular, we suggest that the maximum order of the polynomial, or more generally the library of functions to fit, need to be specified based on visual inspection of the drift/diffusion plots in conjunction with a theoretical understanding of the system. Our code and documentation contains an extended discussion about this aspect (see tutorial notebook: *Advanced Function Fitting*(Note1)).

Data-driven equation discovery methods present an alternative to empirical dynamic modeling or machine learning approaches that offer *equation-free* models for data (Dietrich *et al.* 2021, Evangelou *et al.* 2022, Pratiush *et al.* 2023). In equation-free approaches, the model is not easily amenable to interpretations but they can help model complex high-dimensional datasets. As a contrast, equation discovery approaches are particularly powerful when we are interested in low-dimensional descriptions of biological systems.

The use of sparse regression for equation-learning can be perceived as somewhat limiting, as it limits the space of functions can be discovered to those representable as linear combinations of the functions in the library (see

*Methods*). However, the default choice of a polynomial basis as the library is suitable for many applications, as demonstrated with two contrasting datasets of cells and fish schools. Even for systems where nonpolynomial approximations are required, a custom library can be specified in PyDaDDy—indeed, this approach was used in some of the models in section *Validation with classical models in theoretical biology* and Appendix B. As an alternative, when more complicated non-linear functions are required, the jump moment discovery in PyDaDDy can be combined with other equation discovery techniques such as *symbolic regression* (Cranmer 2023).

Like the machine learning methods, our approach too requires sufficiently good quality data — in particular, highly temporally resolved and long datasets. This raises the obvious question: how finely resolved and how long a time series is necessary? As shown previously (Jhawar and Guttal 2020), the time series must be at around an order of magnitude (or more) finely resolved than the autocorrelation time of the state variable. When the time resolution is comparable or more than the autocorrelation time, the dynamics of the system can't be captured; for such coarse time series, the estimated drift and diffusion functions typically converge to linear and upward-parabolic functions, independent of the actual dynamics (Rinn *et al.* 2016, Riera and Anteneodo 2010). While we are not aware of any studies that have looked at the *minimum length* required to estimate the drift and diffusion reliably, based on our numerical simulations of models shown in this study (Appendix C), we speculate that the total length must be at least a few orders of magnitude times the length of the autocorrelation time. In addition, we need time series data that sufficiently explores the full phase-space of the system. For instance, if a system with multiple stable states is stuck near one of its stable points, we may not be able to discover a model that correctly captures the full phase portrait. This can happen if the time series is short, or if the noise strength is too small. However, this limitation can be readily overcome in systems where experimental manipulations are feasible: Here, one can design different treatments of experiments that begin at different locations of the state-space and run the systems for relatively short periods of time. Each of those treatments may reach a locally stable state and length of time series from each such treatment will be short. However, by putting them all together, one can obtain the stochastic dynamical equation, as we have shown for synthetic datasets in Appendix B.

*Related work* To the best of our knowledge, there is no other comparable package that offers a comprehensive solution for discovering, examining and diagnosing SDE models from time series data. In addition to discovering interpretable SDEs from data, PyDaDDy also integrates comprehensive visualization and diagnostic tools, making a *one-stop-shop* solution for data-driven SDE modelling for empiricists seeking to do this type of modeling. Such detailed visualization and diagnostic

tools are often missing in comparable modeling tools. For completeness, below we provide a detailed qualitative comparison between PyDaDDy and related code bases.

As detailed in the *Methods* section, PyDaDDy takes an *equation learning* approach to discover an interpretable SDE from data. Equation learning is a novel technique, first introduced in the engineering literature in the context of ordinary and partial differential equations, and is implemented in the popular packages like *PySINDy* (de Silva *et al.* 2020) and *DataDrivenDiffEq.jl* (JuliusMartensen *et al.* 2021). These packages, however, are restricted to discovering *deterministic* differential equations.

The R package *Langevin* (Rinn *et al.* 2016) takes a (one or two dimensional) time series as an input and estimates the drift and diffusion functions as bin-wise averaged Kramer-Moyal coefficients. Some functionality is provided for visualizing and diagnosing the estimated coefficients. However, bin-wise averaged estimates can often be error-prone (Jhawar and Guttal 2020, Callahan *et al.* 2021) especially when dealing with limited data (see Appendix C)—this issue is largely mitigated in our equation learning approach. More recently, the Python package *KramersMoyal* (Gorjão and Meirinhos 2019) improves upon estimation issues by imposing smoothness constraints (using kernel density estimation) for drift and diffusion estimation. This package works with arbitrary dimensional time series. Nevertheless, neither of these packages produce an interpretable expression for the SDE; and diagnostic tools are either limited (*Langevin*) or not available (*KramersMoyal*).

Other packages, such as *DiffEqParamEstim.jl* (Rackauckas and Nie 2017) and *Sim.DiffProc* (Guidoum and Boukhetala 2020) take a different approach, where the SDE is estimated using *parameter estimation*. These codes require the user to specify a parametric form of the drift and diffusion functions. Thus, they can be used only when the user knows *a priori* what the functional form of the SDE is; and cannot be used to discover equations from entirely novel time series data. For example, these packages cannot *discover* the fact that the time series in Fig. 2A-*i* and Fig. 2A-*ii* come from fundamentally differing dynamical models.

Importantly, PyDaDDy includes comprehensive diagnostic and visual tools which are either limited or absent in other packages. Specifically, we have incorporated three levels of diagnostics: (i) noise diagnostics, (ii) model diagnostics, and (iii) the model consistency, proposed by (Jhawar and Guttal 2020). Finally, we have also demonstrated the applicability of our package using real-world datasets: something that is typically missing from other packages.

## CONCLUSION

We are making rapid headway towards collecting large datasets in biological systems across scales. As the era of big data looms over biology, we hope that our presentation of a method together with a relatively easy to use package – that helps one characterise the governing dynamical equations from the data – will inspire usage of these methods in the field. These methods present substantial advance in comparison to conventional statistical modelling techniques; while the latter merely estimate parameters of user defined functions, the former can discover symbolic model expressions, thus offering potential explanatory and mechanistic insights to biological datasets. Secondly, when combined with the ability to discover stochastic dynamical models, we can exploit the potential for mechanistic predictive models while accounting for inherent stochasticities of the systems. We expect many challenges, and hence opportunities for future work, when applying these methods to other complex real world datasets that may be high-dimensional, driven by changing parameters and more complicated noise structures.

## METHODS

### Discovering interpretable drift and diffusion functions

Consider a  $d$ -dimensional state variable  $\mathbf{x}$ , observed at some sampling interval  $\Delta t$ . Assuming that the time series was generated by an underlying SDE  $\dot{\mathbf{x}} = \mathbf{f}(\mathbf{x}) + \mathbf{g}(\mathbf{x}) \cdot \boldsymbol{\eta}$ , we define *instantaneous* drift and diffusion (also known as the Kramer Moyal coefficients), as a function of  $t$  and the instantaneous value of the state variable  $\mathbf{x}$ , as:

$$\tilde{F}(t; \mathbf{x}) = \frac{\mathbf{x}(t + \Delta t) - \mathbf{x}(t)}{\Delta t} \quad (11)$$

$$\tilde{G}(t; \mathbf{x}) = \frac{(\mathbf{x}(t + \Delta t) - \mathbf{x}(t))(\mathbf{x}(t + \Delta t) - \mathbf{x}(t))^T}{\Delta t} \quad (12)$$

Since  $x$  is  $d$ -dimensional,  $\tilde{F}$  is a  $d \times 1$  vector and  $\tilde{G}$  is a  $d \times d$  matrix. From these instantaneous drift and diffusion functions  $\tilde{F}$  and  $\tilde{G}$ , respectively, we find interpretable mathematical expressions for each of the components of  $F$  and  $G$  following the approach of Brunton et. al. (Brunton *et al.* 2016). Briefly, we start with a *library* of candidate terms and use sparse regression to fit each of the components of  $F$  or  $G$ , independently, as a linear combination of a small number of terms from the library.

Specifically, consider a *library* of candidate functions  $\{F_1, F_2, \dots, F_k\}$ . For instance,  $F_i$  could be monomials up to a specified degree, another suitable basis such as a Fourier or Chebyshev basis, or domain-specific basic functions tailored for the problem. We wish to represent the drift function  $F$  as a linear combination of only a few

of these candidate functions. In other words, we would like to find coefficients  $\xi_i$  such that  $F(x) = \sum_i \xi_i F_i(x)$  such that only a few of the  $\xi_i$ 's are nonzero. This can be achieved using sparse regression, as detailed in the next section.

Note that we use uppercase  $F$  and  $G$  to represent the estimated drift and diffusion to distinguish them from the actual  $\mathbf{f}$  and  $\mathbf{g}$ . The estimated  $F$  corresponds to  $\boldsymbol{\phi}$ , and  $G$  corresponds to  $\mathbf{g}\mathbf{g}^T$ .

### Sparse regression framework for discovering drift and diffusion functions

Following (Brunton *et al.* 2016), we pose the problem of discovering analytical expressions for drift and diffusion as a sparse regression problem. Here, we discuss the details of the sparse regression procedure for the drift function in the scalar case,  $d = 1$  (the procedure for the diffusion function is identical).

Let  $\mathbf{x}_{T \times 1}$  be a column vector containing the state variable  $x$  sampled at each point of time, i.e.  $\mathbf{x}_i = x(i\Delta t)$ .  $T$  is the total number of observations. Let  $\boldsymbol{\phi}_{T \times 1}$  be a column vector containing the instantaneous drift values, i.e.  $\phi_i = \tilde{F}(i\Delta t)$ . We have a library of candidate functions  $\{F_1, F_2, \dots, F_k\}$  for the drift function. Define a *dictionary matrix*  $\Theta_{T \times k}$  with  $i$ th column given by  $\Theta_i = F_i(\mathbf{x})$ . The notation  $F_i(\mathbf{x})$  is used as shorthand for evaluating  $F_i$  on each entry of  $\mathbf{x}$ . In terms of  $\boldsymbol{\phi}$  and  $\Theta$ , the sparse regression problem corresponds to finding a sparse vector  $\boldsymbol{\xi}$  that solves the equation

$$\boldsymbol{\phi} = \Theta \boldsymbol{\xi} \quad (13)$$

To find a sparse solution for  $\boldsymbol{\xi}$ , we use a procedure called *sequentially thresholded least squares* (STLSQ). The algorithm works as follows: first, a solution for  $\boldsymbol{\xi}$  is found using ordinary least-squares. Now, all entries of  $\boldsymbol{\xi}$  less than a pre-specified *sparsity threshold* are set to 0, and the corresponding columns are removed from the dictionary  $\Theta$ . The procedure is now repeated with the remaining terms, until no more terms can be eliminated.

For the case corresponding to  $d > 1$ , we repeat the above procedure for each of the  $d$  components of  $\tilde{F}$  and  $d^2$  components of  $\tilde{G}$ . One can use the symmetric nature of  $G$  and estimate  $d(d-1)/2$  unique terms.

### Model selection for sparse regression

The sparsity threshold in the STLSQ algorithm is an operational parameter that needs to be chosen appropriately to ensure that the right models are recovered. For different values of the sparsity threshold, we will get different models, and we need to use some criterion to choose the threshold that produces the best model. One approach is to use an appropriate information criterion,

like Akaike Information Criterion (AIC): the model for which the information criterion in minimum is the one that achieves the best trade-off between model fit and model complexity.

An alternate approach, popular in the machine learning literature, is to choose the ideal model based on cross-validated accuracy (Shalev-Shwartz and Ben-David 2014). We choose this approach, and use *k-fold cross validation* for model selection, which we briefly describe here.

The key idea behind cross-validation is to train a model using only part of the data, called *training set*, and evaluate the model performance on a *validation set*, different from the training set. A model that performs well on the validation set will not have overfit on the noise in the training data, and may be more generalisable. Specifically, the dataset is divided into  $k$  equal chunks.  $k - 1$  of the chunks are used as the *training set* to fit the model, with the remaining chunk designated as the *validation set*. The error of the model on the validation set, called the *validation error*, is now computed. The process is repeated with each of the  $k$  chunks designated as the validation set, and the average validation error is computed. The model that gives the minimum cross-validation error is chosen as the best model.

However, since model parsimony is crucial in our application, the model with the minimum cross validation error may not always be the best choice, as non-sparse models may sometimes end up getting selected. To avoid this, we instead sort the models in increasing order of complexity, and choose the model that achieves the *maximum drop* in cross-validation error from the previous model. Here, model complexity is defined simply as the number of terms with non-zero coefficients in the model.

For real-world systems, it is possible to incorporate some understanding of the physics of the system to do the model selection manually; to obtain better and more parsimonious models. We discuss this in more detail in the sections below (D A and B).

### Contrast to conventional approaches

Conventionally, the drift and diffusion as a function of  $\mathbf{x}$  are computed using the respective conditional moments. The drift (respectively, diffusion) at  $\tilde{\mathbf{x}}$  can be approximated as

$$F(\tilde{\mathbf{x}}) = \left\langle \tilde{F}(t; \mathbf{x}) \right\rangle_{\mathbf{x}(t) \in [\mathbf{x}, \mathbf{x} + \epsilon]} \quad (14)$$

$$G(\tilde{\mathbf{x}}) = \left\langle \tilde{G}(t; \mathbf{x}) \right\rangle_{\mathbf{x}(t) \in [\mathbf{x}, \mathbf{x} + \epsilon]} \quad (15)$$

where the angular brackets indicate time averaged value of  $\tilde{F}(t; \mathbf{x})$  (respectively,  $\tilde{G}(t)$ ), computed for all time instances when  $\mathbf{x}$  is within a small bin of width  $\epsilon$  around  $\tilde{\mathbf{x}}$ .

In this conventional approach, the accuracy of the estimated functions  $F$  and  $G$  depends on the sampling interval  $\Delta t$ . There is a bias-variance trade-off at play: smaller values of  $\Delta t$  gives estimates with smaller bias and higher variance, and vice versa. Therefore, subsampling the available time series with a larger  $\Delta t$  is sometimes required to get an optimal estimate ((Jhawar and Guttal 2020), Appendix C).

A crucial point to note is that the bin-wise averaging step (Eq. 14, 15) is not required for the sparse regression: regression can be performed on the instantaneous drift and diffusion (Eq. 11, 12) directly. This eliminates the bin-width parameter  $\epsilon$  from the estimation procedure. In addition, when using sparse regression, there is no need for subsampling the time series, as opposed to bin-wise averaging which requires an optimal choice of  $\Delta t$ .

We re-emphasize that our approach that combines sparse regression with the instantaneous drift and diffusion allowed us to eliminate two arbitrary parameter choices (namely, the bin width and the subsampling time scale) from the estimation procedure.

### Advanced diagnostics

The *Results* section (subsection *Diagnostics*) of the main text discussed several diagnostic tests that can be used to validate the discovered SDE model. More advanced diagnostic tests are also available, which test for further assumptions involved in modelling a stochastic process using an SDE. Some of these are implemented in the PyDaddy package, and are described below:

- Recall that the residuals, defined as  $r(t) = [\dot{x}(t) - F(x(t))] / \sqrt{G(x(t))}$  are an estimate for the noise  $\eta(t)$ , and should have a standard normal distribution. The deviation of the distribution of  $r(t)$  from the standard normal distribution can be examined using a QQ-plot.
- *Pawula's Theorem*: Pawula's theorem states that the third and higher-order Kramers-Moyal (KM) coefficients should be zero, if a process can be modelled using an SDE (Gardiner 2009). In practical scenarios where we have finite-length time series sampled at a finite sampling time, the alternative to Pawula's theorem is that  $K_4(x) \approx 3 \cdot K_2(x)^2$ , where  $K_2$  and  $K_4$  are the second and fourth KM coefficients respectively. (Tabar 2019, Lehnertz et al. 2018).

SDEs discovered from real-world datasets may not always satisfy all these diagnostic tests. For descriptive models, it is often satisfactory if the model passes the simple noise and model diagnostic tests mentioned in the *Results* section (subsection *Diagnostics*). However, for quantitative applications where predictive accuracy is important, one has to ensure that all the assumptions behind SDE models are met—hence, the advanced diagnostic tests mentioned here become crucial.

## CODE AND DATA AVAILABILITY

The code for data-driven SDE discovery is available as a Python package at <https://github.com/tee-lab/PyDaddy>, along with detailed documentation and tutorials at <https://pydaddy.readthedocs.io>. Several tutorial notebooks are provided at <https://pydaddy.readthedocs.io/en/latest/tutorials.html> to familiarise the user with the package.

The fish schooling dataset is from (Jhawar *et al.* 2020), and is available at <https://doi.org/10.5281/zenodo.3596324>. A subset of this dataset as provided as sample data with the package.

The cell migration dataset is from (Brückner *et al.* 2019). The dataset is provided as sample data with the package.

## ACKNOWLEDGEMENTS

VG acknowledges support from the Science and Engineering Research Board, Department of Biotechnology, CEFIPRA and DST-FIST. DRM acknowledges support from the DST INSPIRE Faculty Award. JJ acknowledges support from the Humboldt Postdoctoral Fellowship and the Heidelberger Akademie der Wissenschaften, Heidelberg, Germany. DBB acknowledges support from

the NOMIS foundation and the EMBO Postdoctoral fellowship (ALTF 343-2022). AN and SP acknowledge support from the MoE PhD Fellowship. The authors thank Ashrit Mangalwedhekar, Vivek Jadhav, Shikhara Bhat, Cassandre Aimon and Harishankar Muppurala for comments on the manuscript and code.

## AUTHOR CONTRIBUTIONS

*Arshed Nabeel* Data curation, Formal analysis, Investigation, Methodology, Software, Visualization, Writing (Original Draft Preparation), Writing (Review and Editing)

*Ashwin Karichannavar* Data curation, Formal analysis, Investigation, Methodology, Software

*Shuaib Palathingal* Formal analysis, Investigation, Validation

*Jitesh Jhawar* Data curation, Investigation

*David Brückner* Data curation, Investigation

*Danny Raj M* Conceptualization, Project Administration, Validation, Writing (Original Draft Preparation), Writing (Review and Editing)

*Vishwesha Guttal* Conceptualization, Funding acquisition, Project Administration, Resources, Supervision, Validation, Writing (Original Draft Preparation), Writing (Review and Editing)

S. H. Strogatz, *Nonlinear dynamics and chaos: with applications to physics, biology, chemistry, and engineering* (CRC press, 2018).

N. J. Gotelli *et al.*, *A primer of ecology*, Vol. 494 (Sinauer Associates Sunderland, MA, 2008).

A. J. McKane and T. J. Newman, Stochastic models in population biology and their deterministic analogs, *Physical Review E* **70**, 041902 (2004).

H. Cheng, N. Yao, Z.-G. Huang, J. Park, Y. Do, and Y.-C. Lai, Mesoscopic interactions and species coexistence in evolutionary game dynamics of cyclic competitions, *Scientific Reports* **4**, 1 (2014).

C. A. Yates, R. Erban, C. Escudero, I. D. Couzin, J. Buhl, I. G. Kevrekidis, P. K. Maini, and D. J. T. Sumpter, Inherent noise can facilitate coherence in collective swarm motion, *Proceedings of the National Academy of Sciences* **106**, 5464 (2009).

M. Loreau, From populations to ecosystems, in *From Populations to Ecosystems* (Princeton University Press, 2010).

R. Durrett and S. Levin, The importance of being discrete (and spatial), *Theoretical population biology* **46**, 363 (1994).

T. Biancalani, L. Dyson, and A. J. McKane, Noise-induced bistable states and their mean switching time in foraging colonies, *Physical review letters* **112**, 038101 (2014).

J. Jhawar, R. G. Morris, and V. Guttal, Deriving Mesoscopic Models of Collective Behavior for Finite Populations, in *Handbook of Statistics*, Vol. 40 (Elsevier, 2019) pp. 551–594.

S. Majumder, A. Das, A. Kushal, S. Sankaran, and V. Guttal, Finite-size effects, demographic noise, and ecosystem dynamics, *The European Physical Journal Special Topics* **230**, 3389 (2021).

S. Leyk, A. E. Gaughan, S. B. Adamo, A. de Sherbinin, D. Balk, S. Freire, A. Rose, F. R. Stevens, B. Blankespoor, C. Frye, *et al.*, The spatial allocation of population: a review of large-scale gridded population data products and their fitness for use, *Earth System Science Data* **11**, 1385 (2019).

R. Nathan, C. T. Monk, R. Arlinghaus, T. Adam, J. Alós, M. As-saf, H. Baktoft, C. E. Beardsworth, M. G. Bertram, A. I. Bjåleveld, *et al.*, Big-data approaches lead to an increased understanding of the ecology of animal movement, *Science* **375**, eabg1780 (2022).

J. Jhawar, R. G. Morris, U. Amith-Kumar, M. Danny Raj, T. Rogers, H. Rajendran, and V. Guttal, Noise-induced schooling of fish, *Nature Physics* **16**, 488 (2020).

K. Tunstrøm, Y. Katz, C. C. Ioannou, C. Huepe, M. J. Lutz, and I. D. Couzin, Collective states, multistability and transitional behavior in schooling fish, *PLoS computational biology* **9**, e1002915 (2013).

N. C. Stenseth, W. Falck, O. N. Bjørnstad, and C. J. Krebs, Population regulation in snowshoe hare and canadian lynx: asymmetric food web configurations between hare and lynx, *Proceedings of the National Academy of Sciences* **94**, 5147 (1997).

O. N. Bjørnstad and B. T. Grenfell, Noisy clockwork: time series analysis of population fluctuations in animals, *Science* **293**, 638 (2001).

R. E. Lenski, Experimental evolution and the dynamics of adaptation and genome evolution in microbial populations, *The ISME journal* **11**, 2181 (2017).

S. R. Carpenter, B. M. Arani, P. C. Hanson, M. Scheffer, E. H. Stanley, and E. Van Nes, Stochastic dynamics of cyanobacteria



- in long-term high-frequency observations of a eutrophic lake, *Limnology and Oceanography Letters* **5**, 331 (2020).
- Y. Xie, Z. Sha, and M. Yu, Remote sensing imagery in vegetation mapping: a review, *Journal of plant ecology* **1**, 9 (2008).
- S. Majumder, K. Tamma, S. Ramaswamy, and V. Guttal, Inferring critical thresholds of ecosystem transitions from spatial data, *Ecology* **100**, e02722 (2019).
- W. Horsthemke and R. Lefever, Noise-induced transitions, *Noise in nonlinear dynamical systems* **2**, 179 (1989).
- P. D’Odorico, F. Laio, and L. Ridolfi, Noise-induced stability in dryland plant ecosystems, *Proceedings of the National Academy of Sciences* **102**, 10819 (2005).
- J. Gradišek, S. Siegert, R. Friedrich, and I. Grabec, Analysis of time series from stochastic processes, *Physical Review E* **62**, 3146 (2000).
- R. Friedrich, J. Peinke, M. Sahimi, and M. R. R. Tabar, Approaching complexity by stochastic methods: From biological systems to turbulence, *Physics Reports* **506**, 87 (2011).
- R. Tabar, *Analysis and data-based reconstruction of complex nonlinear dynamical systems*, Vol. 730 (Springer, 2019).
- J. Jhawar and V. Guttal, Noise-induced effects in collective dynamics and inferring local interactions from data, *Philosophical Transactions of the Royal Society B* **375**, 20190381 (2020).
- P. Rinn, P. G. Lind, M. Wächter, and J. Peinke, The Langevin Approach: An R Package for Modeling Markov Processes, *Journal of Open Research Software* **4**, 10.5334/jors.123 (2016).
- S. L. Brunton, J. L. Proctor, and J. N. Kutz, Discovering governing equations from data by sparse identification of nonlinear dynamical systems, *Proceedings of the national academy of sciences* **113**, 3932 (2016).
- S. H. Rudy, S. L. Brunton, J. L. Proctor, and J. N. Kutz, Data-driven discovery of partial differential equations, *Science advances* **3**, e1602614 (2017).
- B. M. de Silva, K. Champion, M. Quade, J.-C. Loiseau, J. N. Kutz, and S. L. Brunton, Pysindy: A python package for the sparse identification of nonlinear dynamical systems from data, *Journal of Open Source Software* **5**, 2104 (2020).
- L. Boninsegna, F. Nüske, and C. Clementi, Sparse learning of stochastic dynamic equations, *The Journal of Chemical Physics* **148**, 241723 (2018), arXiv: 1712.02432.
- Y. Huang, Y. Mabrouk, G. Gompper, and B. Sabass, Sparse inference and active learning of stochastic differential equations from data, arXiv preprint arXiv:2203.11010 10.48550/arXiv.2203.11010 (2022).
- J. L. Callahan, J.-C. Loiseau, G. Rigas, and S. L. Brunton, Non-linear stochastic modelling with langevin regression, *Proceedings of the Royal Society A* **477**, 20210092 (2021).
- A. Frishman and P. Ronceray, Learning force fields from stochastic trajectories, *Physical Review X* **10**, 021009 (2020).
- D. B. Brückner, P. Ronceray, and C. P. Broedersz, Inferring the dynamics of underdamped stochastic systems, *Physical review letters* **125**, 058103 (2020).
- C. Gardiner, *Stochastic methods*, Vol. 4 (springer Berlin, 2009).
- D. B. Brückner, A. Fink, C. Schreiber, P. J. Röttgermann, J. O. Rädler, and C. P. Broedersz, Stochastic nonlinear dynamics of confined cell migration in two-state systems, *Nature Physics* **15**, 595 (2019).
- S. R. Carpenter, D. Ludwig, and W. A. Brock, Management of eutrophication for lakes subject to potentially irreversible change, *Ecological applications* **9**, 751 (1999).
- D. Alonso, F. Bartumeus, and J. Catalan, Mutual interference between predators can give rise to Turing spatial patterns, *Ecology* **83**, 28 (2002).
- T. Vicsek and A. Zafeiris, Collective motion, *Physics reports* **517**, 71 (2012).
- J. Toner, Y. Tu, and S. Ramaswamy, Hydrodynamics and phases of flocks, *Annals of Physics* **318**, 170 (2005).
- S. Ramaswamy, Active matter, *Journal of Statistical Mechanics: Theory and Experiment* **2017**, 054002 (2017).  
<https://pydaddy.readthedocs.io/en/latest/tutorials.html#advanced-function-fitting>.
- F. Dietrich, A. Makeev, G. Kevrekidis, N. Evangelou, T. Bertalan, S. Reich, and I. G. Kevrekidis, Learning effective stochastic differential equations from microscopic simulations: combining stochastic numerics and deep learning, arXiv:2106.09004 [physics] 10.48550/arXiv.2106.09004 (2021), arXiv: 2106.09004.
- N. Evangelou, F. Dietrich, J. M. Bello-Rivas, A. Yeh, R. Stein, M. A. Bevan, and I. G. Kevrekidis, Learning Effective SDEs from Brownian Dynamics Simulations of Colloidal Particles, arXiv:2205.00286 [cs, math] 10.48550/arXiv.2205.00286 (2022), arXiv: 2205.00286.
- U. Pratiush, A. Nabeel, V. Guttal, and P. AP, Discovering mesoscopic descriptions of collective movement with neural stochastic modelling, arXiv preprint arXiv:2303.09906 (2023).
- M. Cranmer, Interpretable machine learning for science with pysr and symbolicregression. jl, arXiv preprint arXiv:2305.01582 (2023).
- R. Riera and C. Anteneodo, Validation of drift and diffusion coefficients from experimental data, *Journal of Statistical Mechanics: Theory and Experiment* **2010**, P04020 (2010).
- JuliusMartensen, C. Rackauckas, *et al.*, Datadrivendiffeq.jl (2021).
- L. R. Gorjão and F. Meirinhos, kramersmoyal: Kramers–moyal coefficients for stochastic processes, *Journal of Open Source Software* **4**, 1693 (2019).
- C. Rackauckas and Q. Nie, Differentialequations.jl – a performant and feature-rich ecosystem for solving differential equations in julia, *The Journal of Open Research Software* **5** (2017), exported from <https://app.dimensions.ai> on 2019/05/05.
- A. C. Guidoum and K. Boukhetala, Performing parallel monte carlo and moment equations methods for itô and stratonovich stochastic differential systems: R package sim.diffproc, *Journal of Statistical Software* **96**, 1–82 (2020).
- S. Shalev-Shwartz and S. Ben-David, *Understanding machine learning: From theory to algorithms* (Cambridge university press, 2014).
- K. Lehnertz, L. Zabawa, and M. R. R. Tabar, Characterizing abrupt transitions in stochastic dynamics, *New Journal of Physics* **20**, 113043 (2018).
- A. Nabeel, V. Jadhav, D. R. Masila, C. Sire, G. Theraulaz, R. Escobedo, S. Iyer, and V. Guttal, Data-driven discovery of stochastic dynamical equations of collective motion, *Physical Biology* (2023).

## Appendix A: The PyDaDDy Package: A brief introduction

We implement our technique for data-driven SDE discovery as a Python package, **PyDaDDy** (Python library for **Data Driven Dynamics**). PyDaDDy takes either a scalar or 2-dimensional vector time series as input. Although the theory of jump moment estimation and equation learning applies to arbitrary dimensions, visualising and diagnosing results becomes infeasible for dimensions larger than two. Therefore, we choose to limit the functionality of the package to dimensions up to two.

From a given uniformly sampled 1-D or 2-D time series, PyDaDDy can compute, visualise, and fit drift and diffusion functions. PyDaDDy also supports time series with missing data points. Diagnostic tools are provided to verify whether the assumptions necessary for modelling the time series as an SDE are met. Finally, PyDaDDy can export data into a DataFrame or a CSV file. Fig. 1 shows an overview of the package and its various functionalities.

For ease of use, we make the package and the associated tutorial notebooks accessible online, even without installation, via Google Colab: <https://pydaddy.readthedocs.io/en/latest/usage.html#pydaddy-on-google-colab>.

The package can also be installed on a local machine using PIP or Conda:

```
pip install pydaddy
```

or

```
conda install pydaddy -c tee-lab
```

PyDaDDy features a single-command operation mode, which allows the user to run a dataset through PyDaDDy and generate a comprehensive HTML report. This can be done using the command:

```
pydaddy <dataset-file-name>
```

The report contains interactive figures of the estimated drift and diffusion functions (with default parameters and automatic threshold tuning—see below) and diagnostic results about noise statistics and model self consistency.

PyDaDDy also has a comprehensive Python API for advanced usage; which allows the user to individually generate various plots, perform diagnostics, or fine-tune the function fitting procedure.

### Summary figure and estimation of drift and diffusion

The estimation workflow starts by creating a PyDaDDy object `dd`, initialised with a dataset.

```
dd = pydaddy.Characterize([x, y], t=0.12)
```

where `x` and `y` are Numpy arrays of the  $m_x$  and  $m_y$  time series respectively. A summary figure is generated with basic statistics of the time series such as the autocorrelation function and histograms of `m`. The summary figure also shows a preliminary estimate of the drift and diffusion functions, using binwise averaged jump moments (see (Jhawar *et al.* 2020, Jhawar and Guttal 2020) for more details on the binwise averaging method).

### Fitting analytical expressions for drift and diffusion functions

PyDaDDy uses a sparse regression technique for model fitting for the drift and diffusion functions. This can be done using the `fit()` function of the `dd` object. By default, PyDaDDy fits polynomial functions, but other function families can also be fit using custom libraries. A *sparsification threshold*, which governs the number of terms in the fit (see SI Section S1B) can be either chosen automatically using cross-validation (see SI Section S1C), or be set manually.

For example,

```
dd.fit('F1', order=3, tune=True, plot=True)
```

fits a degree-3 polynomial (`order=3`) with sparsification threshold chosen automatically (`tune=True`). The first argument names the function to be fitted: `F1` and `F2` correspond to the two components of the drift; `G11` and `G22` correspond to diffusion, and `G12` and `G21` correspond to cross diffusion. The `plot=True` argument tells the function to produce a cross-validation error plot for a range of thresholds. The ideal threshold should strike a balance between the error and number of terms in this plot. PyDaDDy chooses as high as a threshold as possible without increasing the cross-validation error too much.

The threshold can also be manually set by the user. For example,

```
dd.fit('F1', order=3, threshold=0.1)
```

produces a polynomial with degree up to 3, with only terms with coefficients 0.1 or higher.

### Diagnostics

It is essential to ensure that the assumptions involved in modelling the time series as an SDE are not violated. PyDaDDy provides diagnostic functions to verify that the assumptions involved in modelling a time series as an SDE are met (see *Methods* in the main text). Diagnostic plots in PyDaDDy can be generated using

```
dd.noise_diagnostics()
```

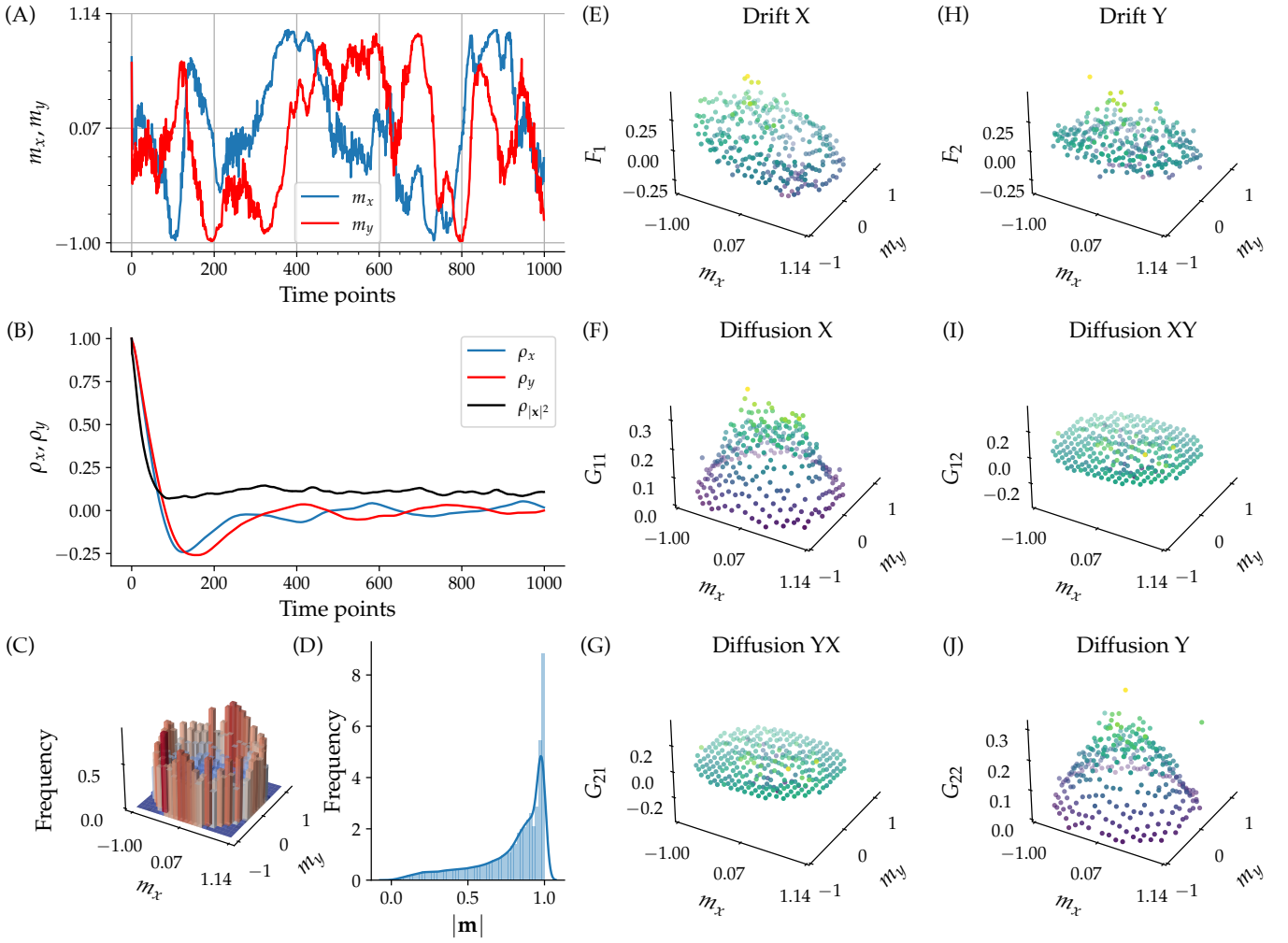


FIG. A1. The summary plot generated by PyDaddy when applied to schooling fish data from the reference (Jhawar *et al.* 2020). (A) Input time series (fish group polarisation), a vector time series denoted by  $\mathbf{m} = (M_x, M_y)$ . One time step corresponds to 0.12 s. (B) Autocorrelation functions of the time series, showing that the autocorrelation decays with time. (C, D) Frequency histograms of time series  $\mathbf{m}$  and  $|\mathbf{m}|$ . (E, H) Preliminary estimates of drift functions. (F, G, I, J) and diffusion functions. The drift and diffusion functions shown here are bin-wise averages of the jump moments (bin-wise averaging is done only for the visualisation).

SI Fig. A2 shows the output of the noise diagnostics for the fish schooling dataset.

In addition, PyDaDDy can also perform a model self-consistency check (see *Methods*) using the following command:

```
dd.model_diagnostics()
```

This function uses the estimated SDE to generate a simulated time series, with the same length and sampling interval as the original dataset. It then estimates the drift and diffusion functions from the simulated time series, using the same order and threshold used in the original estimation. Finally, a summary figure is generated, comparing the histogram, drift and diffusion functions of the original dataset to the simulated dataset (SI Fig. A3). If the model is self-consistent, we expect a good match between the original and the simulated

time series.

## Appendix B: Demonstration with classic models in biology

In this section, we demonstrate the generality of the PyDaddy package with several classical models in theoretical biology and beyond. The models considered are listed below.

*a. Logistic model of population growth.* We consider the logistic model of population growth, with a demographic noise term that grows as the square root of the population size, governed by the following SDE:

$$\dot{N} = 2N \left( 1 - \frac{N}{5} \right) + \sqrt{N} \cdot \eta(t) \quad (\text{B1})$$

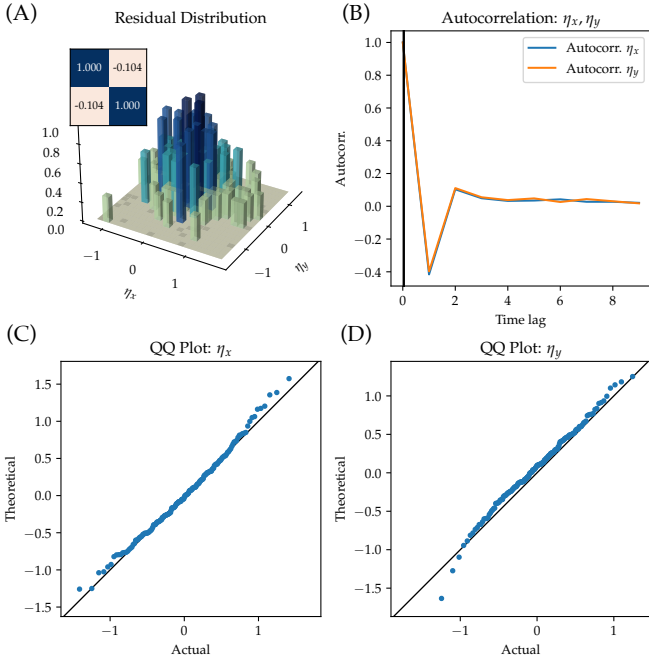


FIG. A2. **Noise diagnostics figure generated by PyDaDDy when applied to schooling fish data from the reference (Jhawar *et al.* 2020)** (A) Distribution of the residuals, which resembles a bivariate Gaussian with zero mean. The inset matrix shows correlation matrix of the  $x$  and  $y$  components of the noise. This should be close to the identity matrix. (B) Autocorrelation functions of the residuals, with the black line marking the autocorrelation time and is close to zero, as desired. (C, D) QQ-plots of the marginal distributions, which nearly falls on a line of slope 1, again as desired by the assumptions of the SDE model.

*b. Harvesting model.* We consider a population growth model with a harvesting term of Holling's Type III form, with a multiplicative noise term.

$$\dot{N} = 2.4N \left(1 - \frac{N}{6}\right) - \frac{4N^2}{1 + N^2} + 0.2 \left(\frac{N^2}{1 + N^2}\right) \cdot \eta(t) \quad (\text{B2})$$

*c. Lake eutrophication model.* We consider a lake eutrophication model (Carpenter *et al.* 1999) with an additive noise term.

$$\dot{x} = 0.5 - x + \frac{x^8}{1 + x^8} + 0.2 \cdot \eta(t) \quad (\text{B3})$$

*d. Lotka-Volterra competition model.* We consider the classical Lotka-Volterra model for inter-species competition.

$$\dot{x} = 2x \left(1 - \frac{1}{6}(x + y)\right) + 0.1x \cdot \eta(t) \quad (\text{B4})$$

$$\dot{y} = 4y \left(1 - \frac{1}{8}(2x + y)\right) + 0.1y \cdot \eta(t) \quad (\text{B5})$$

*e. Van der Pol oscillator.* We considered the Van der Pol model of relaxed, non-linear oscillations, with the velocity dynamics being perturbed by an additive noise term.

$$\dot{x} = v \quad (\text{B6})$$

$$\dot{v} = -x + 5(v + x^2v) + \eta(t) \quad (\text{B7})$$

*f. Prey-predator model.* Finally, we considered a Prey-predator model (Alonso *et al.* 2002) with predation having a Holling's Type II form.

$$\dot{n} = n(n - 1) - \frac{np}{n + p} + 0.1n \cdot \eta(t) \quad (\text{B8})$$

$$\dot{p} = 0.48 \frac{np}{n + p} - 0.2p + 0.1p \cdot \eta(t) \quad (\text{B9})$$

For each model, we generated simulated time series data (of  $10^5$  time points) using the corresponding SDE model using an Euler-Maruyama SDE integration scheme. We then used the simulated time series to estimate SDEs using PyDaDDy. The results of PyDaDDy SDE discovery are given in Table S1.

For the logistic, Lotka-Volterra and Van der Pol models, we used the default polynomial library for fitting, as these are indeed polynomial models. For the other models, we used custom libraries. The library consisted of terms  $x, x^2, x/(x + 1), x^2/(x^2 + 1)$  for the harvesting model,  $1, x, x^2, x^8/(x^8 + 1)$  for the lake eutrophication model,  $n, p, n^2, p^2, np/(n + p)$  for the prey-predator model. For the harvesting and Lotka-Volterra simulations, we generated 10 different simulations with different initial conditions, so that we get a good coverage of the phase space (see *Discussion* section of the main text for more on this point).

For all the models, see that PyDaDDy is able to recover SDEs that closely match the original ground-truth models (Table A1).

We pause here to make a few general notes on constructing a custom library. First, the choice of basis functions in the library should be informed by some knowledge of the underlying physics of the problem. A second and equally important point is that the functions in library should be reasonably orthogonal with respect to each other (i.e., for two functions  $f_1(x)$  and  $f_2(x)$ , the inner product  $\int f_1(x)f_2(x)dx$  should be close 0 over the relevant ranges). If this is not the case, it becomes difficult for regression to disentangle individual contributions of the different functions in the library. For example, for the lake eutrophication model, if the library contains terms  $x^a/(1 + x^a)$  for many different values of  $a$ , all these functions are close to each other and sparse regression may end up representing the harvesting term as a combination of these. A better approach (which we followed in our analysis) would be to try many different fits, each with a library containing only one functional response term, and choose the model with the fit that minimizes the overall error.

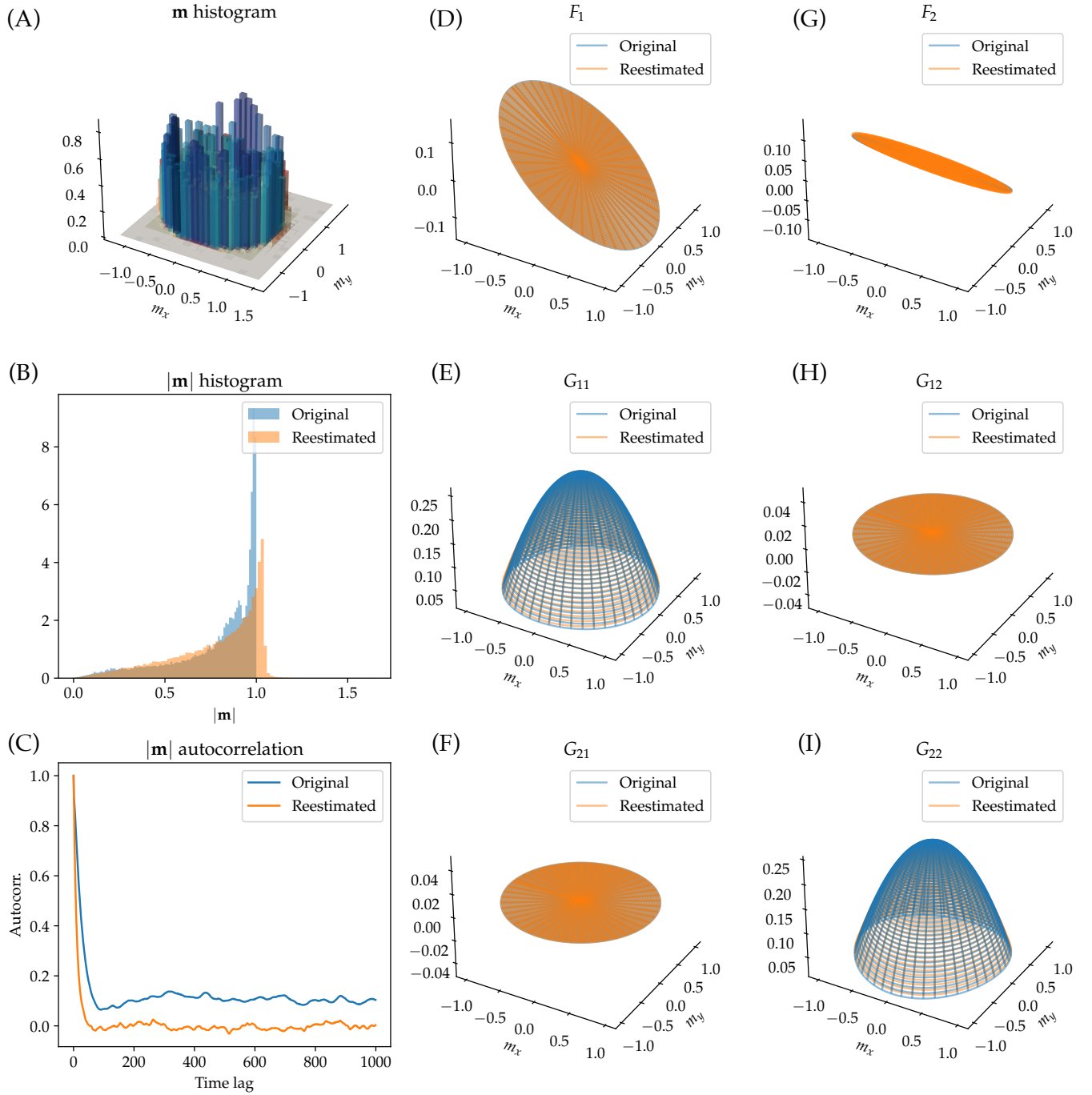


FIG. A3. **Model diagnostics figure generated by PyDaddy when applied to schooling fish data from the reference (Jhawar *et al.* 2020)** (A-B) Comparison of histograms of  $M$  and  $|M|$  respectively, between the original time series and a time series simulated using the discovered SDE. (C) Autocorrelation functions of the simulated time series. (D-I) Comparison of the drift and diffusion functions between the original estimate and re-estimate (from the simulated data).

### Appendix C: Estimation with limited data

In this section, we examine the effects of data limitations on the estimation performance. Two aspects are considered, namely, the length of the time series, and the sampling interval.

### Effect of time series length

In general, one would expect the estimation performance to increase when we have more data. For very short time series, the estimates are noisy and the estimation error is relatively high. As the amount of available

Model	Equations	Estimated Equations
Logistic model	$f(N) = 2N - 0.5N^2$ $g^2(N) = N$	$f(N) = 2.03N - 0.41N^2$ $g^2(N) = 1.07N$
Harvesting model	$f(N) = 2.4N - 0.4N^2 - 4\frac{N^2}{1+N^2}$ $g^2(N) = 0.04\left(\frac{N^2}{1+N^2}\right)^2$	$f(N) = 2.77N - 0.46N^2 - 4.61\frac{N^2}{1+N^2}$ $g^2(N) = 0.04\left(\frac{N^2}{1+N^2}\right)^2$
Lake eutrophication model	$f(x) = 0.5 - x + \frac{x^8}{1+x^8}$ $g^2(x) = 0.04$	$f(x) = 0.53 - 1.05x + 1.06\frac{x^8}{1+x^8}$ $g^2(x) = 0.04$
Lotka-Volterra competition	$f_1(x, y) = 2x - 0.3x^2 + 0.3xy$ $f_2(x, y) = 4y - 0.5y^2 + xy$ $g_{11}^2(x, y) = 0.04x^2$ $g_{22}^2(x, y) = 0.04y^2$	$f_1(x, y) = 2.14x - 0.36x^2 + .38xy$ $f_2(x, y) = 3.99y - 0.49y^2 + 1.02xy$ $g_{11}^2(x, y) = 0.04x^2$ $g_{22}^2(x, y) = 0.04y^2$
Van der Pol	$f_1(x, v) = v$ $f_2(x, v) = -x + 5v - 5x^2v$ $g_{22}^2(x, v) = 25$	$f_1(x, v) = v$ $f_2(x, v) = -1.04x + 4.95v - 4.99x^2v$ $g_{22}^2(x, v) = 25.61$
Prey Predator	$f_1(n, p) = n - n^2 - 1.2\frac{np}{n+p}$ $f_2(n, p) = 0.48\frac{np}{n+p} - 0.2p$ $g_{11}^2(n, p) = 0.01n^2$ $g_{22}^2(n, p) = 0.01p^2$	$f_1(n, p) = 1.02n - 1.03n^2 - 1.22\frac{np}{n+p}$ $f_2(n, p) = 0.49\frac{np}{n+p} - 0.20p$ $g_{11}^2(x, y) = 0.01x^2$ $g_{22}^2(x, y) = 0.01y^2$

TABLE A1. **Reconstructing classical models with PyDaDDy.** Comparison of PyDaDDy reconstructed SDEs with original SDEs for several classical models in biology. Each model is an SDE of the form  $\dot{x} = f(x) + g(x) \cdot \eta(t)$ . For the vector models, the drift  $f$  had components  $f_1(x, y)$  and  $f_2(x, y)$ , and diffusion had components  $g_{11}$ ,  $g_{22}$  (the off-diagonal, cross-diffusion components  $g_{12} = g_{21}$  were 0 for the models considered).

data increases, the estimation error decreases.

Fig. A4 shows the average estimation error, with simulated data of different lengths (ranging from  $10^4$  to  $10^6$  time points), for different models. The averages are computed over 100 different instantiations of each model. As expected, the estimation error for drift decreases with increasing time series length. For diffusion, the estimates are fairly accurate even with short time series, and there is no significant decrease in the estimation error with longer time series.

For comparison, the estimation errors of the bin-wise averaging method are also shown. In general, the estimation errors with the bin-wise averages are much larger than PyDaddy estimation errors. This is due to the fact that the bin-wise approach estimates drift and diffusion functions independently for each bin, and disregards the overall shape and smoothness of the functions. Errors in estimates for individual bins therefore can become quite large when there are only a few samples in the bin. By fitting an analytic function to the jump moments, PyDaddy is able to capture the smoothness of the drift and diffusion functions to achieve better estimates.

### Effect of sampling interval

In the conventional approach of estimating drift and diffusion functions as bin-wise averages, there is a bias-variance trade-off: as the sampling interval increases, the bias in the estimation of drift and diffusion increases, but the variance decreases. To obtain the best trade-off, one may need to subsample the time series at a  $\Delta t$  much larger than the resolution at which the data is available in (Jhavar and Guttal 2020). Fig. A5 shows how, for the bin-wise estimates, the estimation error decreases to a minimum (due to decreasing variance) before starting to increase again as  $\Delta t$  increases. This is due to high variance in the bin-wise estimates for small values of  $\Delta t$ . The effect is particularly evident in the drift estimate.

However, this effect is absent in the sparse regression approach, and smaller  $\Delta t$  always yields smaller estimation errors. The smallest possible  $\Delta t$  (i.e., the temporal resolution at which the data is available in) is usually the best choice for estimation with PyDaddy, further subsampling only decreases estimation performance.



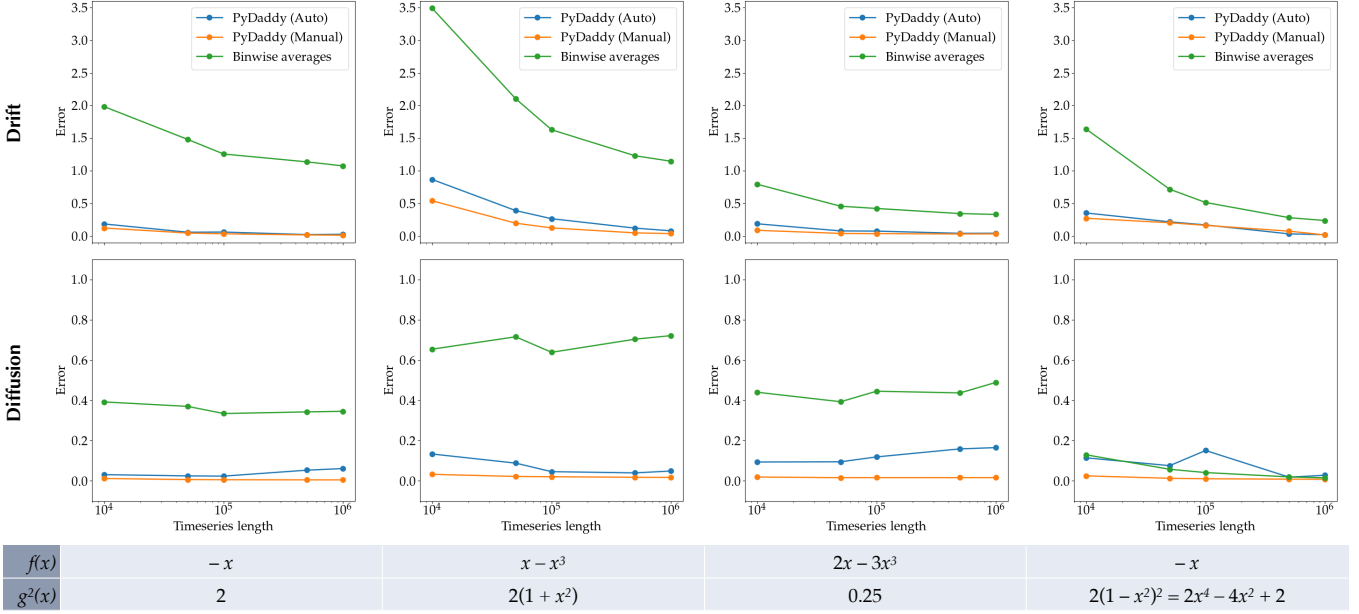


FIG. A4. **Effect of time series length on estimation error.** Estimation errors (relative r.m.s. error) for drift (top) and diffusion (bottom) for four example SDEs. The actual drift and diffusion functions are shown at the bottom. Estimation errors are plotted for conventional bin-wise estimation, PyDaddy estimation with *automatic* threshold tuning, and PyDaddy estimation with *manual* thresholds. In general, as the amount of available data (i.e. time series length) increases, estimation error of drift decreases. Estimation accuracy for diffusion is good even with shorter time series. For both drift and diffusion, PyDaddy achieves much better estimation accuracy than conventional bin-wise averaging, even for short time series.

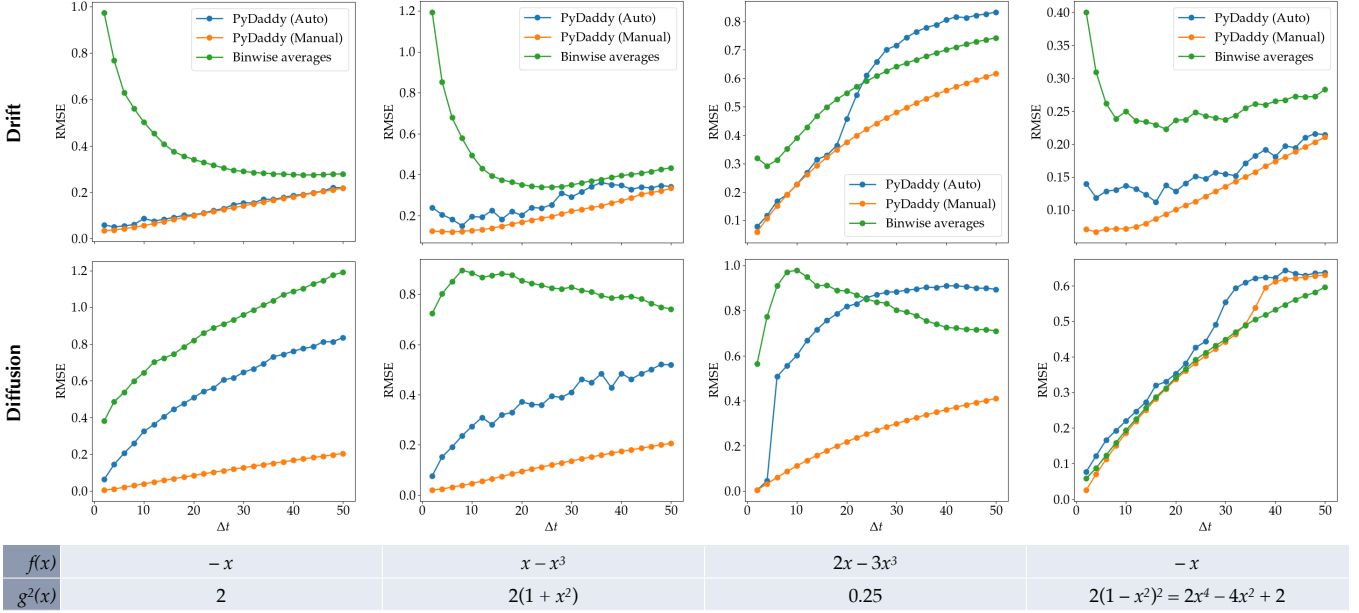


FIG. A5. **Effect of sampling time on estimation error.** Estimation errors (relative r.m.s. error) for drift (top) and diffusion (bottom), as a function of sampling interval  $\Delta t$ , for four example SDEs. The actual drift and diffusion functions are shown at the bottom. Estimation errors are plotted for conventional bin-wise estimation, PyDaddy estimation with automatic threshold tuning, and PyDaddy estimation with manual thresholds. For PyDaddy estimates, the estimation error always increases monotonically with subsampling time  $\Delta t$ . Contrast this with the bin-wise estimates, where the estimation error often has a non-monotonic trend.

## Appendix D: Model selection with real-world datasets

Here, we discuss a typical workflow for discovering data-driven equations from real-world datasets. The process typically involves going back and forth between model discovery and model diagnostics to get the simplest, ‘good enough’ model that captures the essential features of the dynamics. For simplicity, we discuss the procedure in the context of discovering polynomial models.

The model discovery procedure has two *hyperparameters*: the degree of the polynomial, which governs the total number of terms in the library, and the sparsification threshold, which governs how many terms from the library actually end up in the discovered function. Loosely, the model discovery procedure will then have the following steps:

1. Based on visual inspection, the binned drift and diffusion coefficients, choose an appropriate polynomial degree. While there are limitations in using the binned estimates (see *Methods*, section *contrast to conventional approaches*), they serve as a starting point to visualize the structure of the drift and diffusion functions. The fitting procedure does not depend on the binned estimates.
2. Set the sparsification threshold to be 0 (i.e., a polynomial of the specified order with no sparsification will be returned).
3. Generate simulated time series with the discovered models and compare the statistics (histograms and autocorrelation functions) of the simulated time series with the original time series.
4. If the histogram or autocorrelation match sufficiently well, we can conclude that the polynomial degree is high enough to capture the model dynamics. Now, progressively increase the threshold and find the maximum value of threshold (i.e. the sparsest model of the specified degree) that captures the dynamics sufficiently well.
5. If the simulated histogram or autocorrelation do not match the original data, go back to step 1, increase the polynomial degree, and repeat the procedure.
6. Finally, ensure that the chosen model is self consistent. That is, starting with a simulated time series generated with the model, the model discovery procedure should produce the same model.

It is important to note that the cross validation approach to model selection (*Methods*, section *Model selection for sparse regression*) also provides a means to identify a sparse model. However, this is only based on how well the inferred model explains the data that is held back for testing. The manual approach detailed above

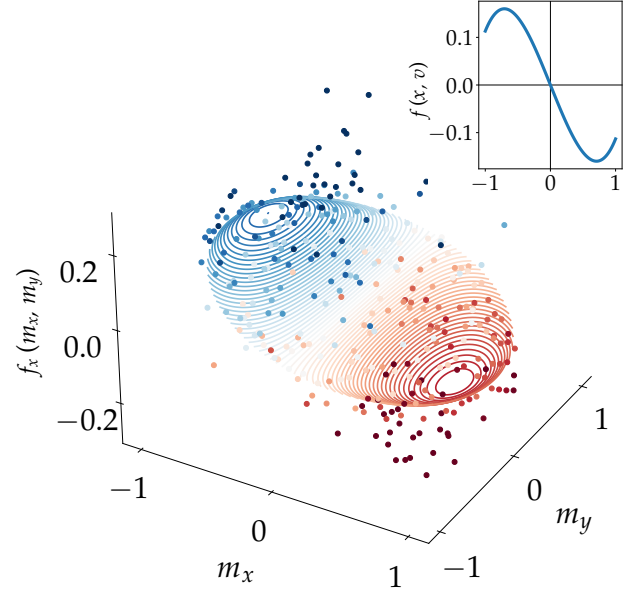


FIG. A6. A cubic function offers a slightly better fit for the drift.

checks for model consistency, and if the model is able to reproduce the histograms and autocorrelation of the state variable, which weren’t used in the identification of the SDE model.

### Model selection for the fish schooling dataset

For the fish schooling dataset,  $\mathbf{m}(t)$  is a vector, so the governing SDE will be a vector SDE. Therefore, the drift is a vector function and  $\mathbf{g}$  is a matrix function. Sparse fitting can be performed on their individual components independently. Note that it is possible to take in to account the inherent symmetries of  $\mathbf{m}$  to constrain the possible terms and directly derive a vector SDE—this procedure is described in more detail in (Nabeel *et al.* 2023).

Based on visual examination, the components of the drift function  $f_x$  and  $f_y$  cross 0 at  $\mathbf{m} = 0$ , the most parsimonious function that captures this being a linear function. On the other hand, the diffusion components  $g_{xx}$  and  $g_{yy}$  have a dome shape, captured by a quadratic. The cross-terms in the diffusion function,  $g_{xy}$  are negligible and can be safely ignored.

Model diagnostics (main text, Fig.3) reveals that the histogram if the simulated time series matches closely with that of the original time series. The autocorrelation matches the decay envelop of the autocorrelation but not the oscillations. The oscillations in the autocorrelation function is caused by the school swimming along the boundary of the tank, and is a superfluous effect we are not interested in capturing in our minimal SDE model. Therefore, we conclude that a model with a linear drift function, quadratic diffusion function and no

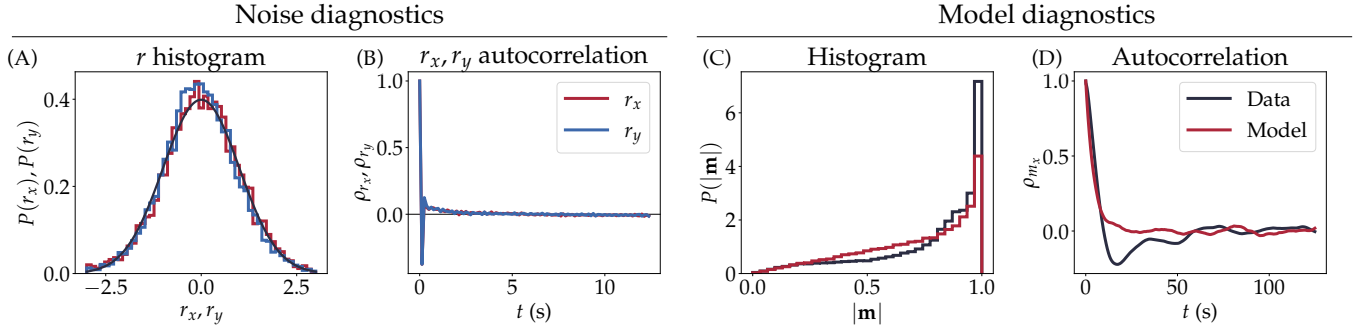


FIG. A7. Noise and model diagnostics, with an SDE model with a cubic drift function. This model offers little to no improvement over an SDE with linear drift.

cross-diffusion terms is sufficient to capture the essential dynamics of the polarisation dynamics of Karimeen fish.

It's worth noting here that a cubic function can give a slightly better fit for the drift function (Fig. A6). However, the cubic function does not change the stability landscape by adding new equilibrium manifold. Furthermore, as shown by the diagnostics (Fig. A6), this model performs no better in terms of replicating the essential statistical features of the data. Therefore, keeping parsimony and model interpretability in mind, we choose the linear drift function over the cubic function.

### Model selection for the cell migration dataset

For the cell migration dataset, only the evolution of  $v$  is governed by an SDE; the position  $x$  simply evolves according to  $\dot{x} = v$ .

Recall that the STLSQ algorithm works by iteratively eliminating coefficients from a discovered function until we reach a minimal model. This procedure works correctly only when all the component variables ( $x$  and  $v$  in this case) are of the same scale. Therefore, as a preprocessing step, we rescale  $x$  and  $v$  to fall between  $-1$  and  $1$  based on the physical constraints of the system. Specifically, we define the non-dimensionalized variables  $\hat{x} = x/x_s$ ,  $\hat{v} = v/v_s$  and  $\hat{t} = t/t_s$  where  $x_s = 50 \mu\text{m}$ ,  $v_s = x_s/\Delta t$  and  $t_s = x_s/v_s$ . ( $\Delta t = 10$  min is the sampling interval.) We can now discover the following dimensionless SDE using the standard STLSQ algorithm:

$$\frac{d\hat{v}}{d\hat{t}} = \hat{f}(\hat{x}, \hat{v}) + \hat{g}(\hat{x}, \hat{v}) \cdot \eta(t) \quad (\text{D1})$$

Based on visual examination, we conjecture that the drift function is of order 3 or higher, while the diffusion is small in magnitude but has a complex shape. We choose a cubic function for the drift and a quartic (4th order) polynomial for the diffusion. This combination is able to generate simulated time series that reasonably match the histograms and autocorrelation functions of

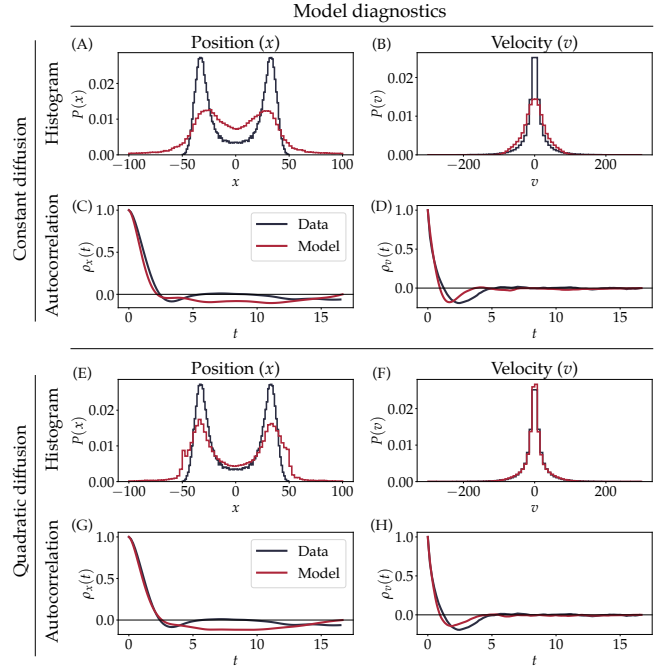


FIG. A8. Model diagnostics for an SDE model for cell migration, with constant, additive noise (A-D) and a quadratic multiplicative noise (E-H). Neither of these models is able to capture the distribution of  $x$  correctly.

$x$  and  $v$  (Fig.5). Note that the the quartic function is essential to characterize the structure of the drift function. Neither a constant additive noise, nor a lower order polynomial function was able to produce a model consistent with the observed distribution of  $x$  (Fig. A8).

Finally, we need to rescale the fitted SDE to the the original, dimensional variables  $x$  and  $v$ . Let the non-dimensional drift and diffusion functions be  $\hat{f}(\hat{x}, \hat{v})$  be  $\hat{g}(\hat{x}, \hat{v})$  respectively. Then, the actual, dimensional  $f$  and  $g$  are given as:

Term	Coeff. in $\hat{f}$	Coeff. in $f$
$x$	-0.035	-1.272
$x^2$	0.038	$5.510 \times 10^{-4}$
$v$	0.083	49.84
$x^2v$	-1.458	$-3.499 \times 10^{-3}$
$xv^2$	-3.723	$-1.489 \times 10^{-3}$
$v^3$	-3.019	$-2.012 \times 10^{-4}$

TABLE A2. The fitted coefficients for the drift function, in the dimensionless coordinates ( $\hat{f}$ ) and the rescaled, dimensional coordinates ( $f$ ).

Term	Coeff. in $\hat{g}^2$	Coeff. in $g^2$
1	0.010	$3.195 \times 10^4$
$x^2$	-0.023	$-1.197 \times 10^{-2}$
$x^4$	0.015	$1.259 \times 10^{-9}$
$xv$	-0.232	$-3.341 \times 10^{-3}$
$x^3v$	0.283	$6.529 \times 10^{-10}$
$v^2$	-0.129	$-5.159 \times 10^{-5}$
$x^2v^2$	1.270	$8.131 \times 10^{-11}$
$xv^3$	1.476	$2.624 \times 10^{-12}$
$v^4$	0.582	$-2.874 \times 10^{-14}$

TABLE A3. The fitted coefficients for the diffusion function, in the dimensionless coordinates ( $\hat{g}^2$ ) and the rescaled, dimensional coordinates ( $g^2$ ).

$$f(x, v) = \frac{v_s}{t_s} \cdot \hat{f} \left( \frac{x}{x_s}, \frac{v}{v_s} \right) \quad (\text{D2})$$

$$g(x, v) = \frac{v_s}{t_s} \cdot \hat{g} \left( \frac{x}{x_s}, \frac{v}{v_s} \right) \quad (\text{D3})$$

Tables A2 and A3 show the coefficients of the estimated drift and diffusion functions, for both the dimensionless and rescaled dimensional coordinates.